In situ investigation of an organic micro-globule and its mineralogical context within a Ryugu “sand” grain

Van T H Phan, Pierre Beck, Rolando Rebois, Eric Quirico, Takaaki Noguchi, Toru Matsumoto, Akira Miyake, Yohei Igami, Mitsutaka Haruta, Hikaru Saito, et al.

In situ investigation of an organic micro-globule and its mineralogical context within a Ryugu "sand" grain

Van T. H. Phan[1*], Pierre Beck[1], Rolando Rebois[1], Eric Quirico[1], Takaaki Noguchi[2,], Toru Matsumoto[2,3], Akira Miyake[2], Yohei Igami[2], Mitsutaka Haruta[4], Hikaru Saito[5,6], Satoshi Hata[7,8], Yusuke Seto[9], Masaaki Miyahara[10], Naotaka Tomioka[11], Hope A. Ishii[12], John P. Bradley[12], Kenta K. Ohtaki[12], Elena Dobrică[12], Hugues Leroux[13], Corentin Le Guillou[13], Damien Jacob[13], Francisco de la Peña[13], Sylvain Laforet[13], Maya Marinova[14], Falko Langenhorst[15], Dennis Harries[16], Neyda M. Abreu[17], Jennifer Gray[18], Thomas Zega[19], Pierre-M. Zanetta[19], Michelle S. Thompson[20], Rhonda Stroud[21], Jérémie Mathurin[22], Alexandre Dazzi[22], Emmanuel Dartois[23], Cécile Engrand[24], Kate Burgess[25], Brittany A. Cymes[26], John C. Bridges[27], Leon Hicks[27,28], Martin R. Lee[29], Luke Daly[29,30,31], Phil A. Bland[32], Michael E. Zolensky[33], David R. Frank[12], James Martinez[34], Akira Tsuchiyama[35,36,37], Masahiro Yasutake[38], Junya Matsuno[35], Shota Okumura[2], Itaru Mitsukawa[2], Kentaro Uesugi[38], Masayuki Uesugi[38], Akihisa Takeuchi[38], Mingqi Sun[36,37,39], Satomi Enju[40], Aki Takigawa[41], Tatsuhiro Michikami[42], Tomoki Nakamura[43], Megumi Matsumoto[43], Yusuke Nakauchi[44], Masanao Abe[44,45], Satoru Nakazawa[44], Tatsuaki Okada[44,45], Takanao Saiki[44], Satoshi Tanaka[44,45], Fuyuto Terui[46], Makoto Yoshikawa[44,45], Akiko Miyazaki[44], Aiko Nakato[44], Masahiro Nishimura[44], Tomohiro Usui[44], Toru Yada[44], Hisayoshi Yurimoto[44], Kazuhide Nagashima[12], Noriyuki Kawasaki[47], Naoya Sakamotoa[48], Peter Hoppe[49], Ryuji Okazaki[50], Hikaru Yabuta[10], Hiroshi Naraoka[50], Kanako Sakamoto[44], Shogo Tachibana[51], Sei-ichiro Watanabe[52], Yuichi Tsuda[44]

[1] Institut de Planétologie et d'Astrophysique de Grenoble (IPAG), Université Grenoble Alpes, CNRS, 38000 Grenoble, France.

[2] Division of Earth and Planetary Sciences, Kyoto University, Kitashirakawaoiwake-cho, Sakyo-ku, Kyoto 606-8502, Japan.

[3]The Hakubi Center for Advanced Research, Kyoto University, Kitashirakawaoiwake-cho, Sakyo-ku, Kyoto 606-8502, Japan

[4]Institute for Chemical Research, Kyoto University, Gokasho, Uji, Kyoto 611-0011, Japan.

[5]Institute for Materials Chemistry and Engineering, Kyushu University, Fukuoka 816-8580, Japan.

[6]Pan-Omics Data-Driven Research Innovation Center, Kyushu University, Fukuoka 816-8580, Japan.

[7]Interdisciplinary Graduate School of Engineering Sciences, Kyushu University, Fukuoka 816-8580, Japan.

[8]The Ultramicroscopy Research Center, Kyushu University, Fukuoka 819-0395, Japan.

[9]Department of Geosciences, Osaka Metropolitan University, Sugimoto 3-3-138, Sumiyoshi-ku, Osaka 558-8585, Japan.

[10]Department of Earth and Planetary Systems Science, Hiroshima University, 1-3-1 Kagamiyama, Higashi-Hiroshima City, Hiroshima, 739-8526, Japan.

[11]Kochi Institute for Core Sample Research, X-Star, JAMSTEC, 200 Monobe Otsu, Nankoku, Kochi 783-8502, Japan.

[12]Hawai'i Institute of Geophysics and Planetology, The University of Hawai'i at Mānoa, 1680 East-West Road, POST Building, Room 602, Honolulu, HI 96822, USA.

[13]Université de Lille, CNRS, INRAE, Centrale Lille, UMR 8207-UMET-Unité Matériaux et Transformations, F-59000 Lille, France.

[14]Université de Lille, CNRS, INRAE, Centrale Lille, Université Artois, FR 2638-IMEC-Institut Michel-Eugène Chevreul, F-59000 Lille, France.

[15]Institut für Geowissenschaften, Friedrich-Schiller-Universität Jena, Carl-Zeiss-Promenade 10, 07745

Jena, Germany.
[16]European Space Resources Innovation Centre, Luxembourg Institute of Science and Technology, 41 rue du Brill, 4422 Belvaux, Luxembourg.
[17]NASA Langley Research Center, Hampton, VA 23681-2199, USA.
[18]Materials Characterization Lab, The Pennsylvania State University Materials Research Institute, Millennium Science Complex, Pollock Road, University Park, PA16802, USA.
[19]Lunar and Planetary Laboratory, Department of Planetary Sciences, The University of Arizona, 1629 E. University Blvd., Tucson AZ 85721-0092, USA.
[20]Department of Earth, Atmospheric and Planetary Sciences, Purdue University, 550 Stadium Mall Drive, West Lafayette, IN 47907-2051, USA.
[21]Buseck Center for Meteorite Studies, Arizona State University, 781 E Terrace Road, Tempe, AZ 85281, USA.
[22]Institut Chimie Physique, Univ. Paris-Saclay, CNRS, 91405 Orsay, France
[23]Institut des Sciences Moléculaires d'Orsay, Univ. Paris-Saclay, CNRS, 91405 Orsay, France
[24]IJCLab, UMR 9012, Univ. Paris-Saclay, CNRS, 91405 Orsay, France
[25]Materials Science and Technology Division, U.S. Naval Research Laboratory, Washington, DC 20375, USA.
[26]NRC Postdoctoral Research Associate, U.S. Naval Research Laboratory, Washington, DC 20375, USA.
[27]Space Park Leicester, The University of Leicester, 92 Corporation Road, Leicester, LE4 5SP, UK.
[28]School of Geology, Geography and the Environment, The University of Leicester, University Road, Leicester, LE1 7RH, UK.
[29]School of Geographical and Earth Sciences, The University of Glasgow, Molema Building, Lilybank Gardens, Glasgow G12 8QQ, UK.
[30]Australian Centre for Microscopy and Microanalysis, The University of Sydney, Sydney, New South Wales, Australia.
[31]Department of Materials, The University of Oxford, Parks Road, Oxford, OX1 3PH, UK.
[32]School of Earth and Planetary Sciences, Curtin University, GPO Box U1987, Perth, Western Australia 6845, Australia.
[33]ARES, NASA Johnson Space Center, 2101 NASA Parkway, Houston, Texas 77058, USA
[34]Jacobs Engineering, 1999 Bryan Street, Suite 1200, Dallas, Texas 75201, USA.
[35]Research Organization of Science and Technology, Ritsumeikan University, 1-1-1 Nojihigashi, Kusatsu, Shiga 525-8577, Japan.
[36]CAS Key Laboratory of Mineralogy and Metallogeny, Guangdong Provincial Key Laboratory of Mineral Physics and Materials, Guangzhou Institute of Geochemistry, Chinese Academy of Sciences (CAS), Guangzhou 510640, China.
[37]CAS Center for Excellence in Deep Earth Science, Guangzhou 510640, China.
[38]Japan Synchrotron Radiation Research Institute, 1-1-1 Kouto, Sayo-cho, Sayo-gun, Hyogo 679-5198, Japan.
[39]University of Chinese Academy of Sciences, Beijing 100049, China.
[40]Department of Mathematics, Physics, and Earth Science, Ehime University, 2-5 Bunkyo-cho, Matsuyama, Ehime 790-8577, Japan.
[41]Department of Earth and Planetary Science, The University of Tokyo, 7-3-1 Hongo, Bunkyo-ku, Tokyo 113-0033, Japan.
[42]Faculty of Engineering, Kindai University, Hiroshima Campus, 1 Takaya Umenobe, Higashi-Hiroshima, Hiroshima 739-2116, Japan.
[43]Department of Earth Science, Tohoku University, 6-3 Aoba, Aramaki, Aoba-ku, Sendai 980-8578, Japan.

[44]Institute of Space and Astronautical Science, Japan Aerospace Exploration Agency, 3-1-1 Yoshinodai, Chuo-ku, Sagamihara, Kanagawa 252-5210, Japan.
[45]The Graduate University for Advanced Studies, SOKENDAI, Hayama 240-0193, Japan.
[46]Department of Mechanical Engineering, Kanagawa Institute of Technology, Atsugi 243-0292, Japan.
[47]Department of Earth and Planetary Sciences, Hokkaido University, Kita-10 Nishi-8, Kita-ku, Sapporo 060-0810, Japan.
[48]Creative Research Institution Sousei, Hokkaido University, Kita-21, Nishi-10, Kita-ku, Sapporo 001-0021, Japan.
[49]Nano- und Mikropartikelforschung, Max Planck Institut für Chemie, Hahn-Meitner-Weg 1, 55128 Mainz, Germany.
[50]Department of Earth and Planetary Sciences, Kyushu University, 744 Motooka, Nishi-ku, Fukuoka 819-0395, Japan.
[51]UTokyo Organization for Planetary and Space Science, The University of Tokyo, 7-3-1 Hongo, Bunkyo-ku, Tokyo 113-0033, Japan.
[52]Department of Earth and Environmental Sciences, Nagoya University, Furo-cho, Chikusa-ku, Nagoya 464−8601, Japan.

[*]Corresponding author. Email: thi-hai-van.phan@univ-grenoble-alpes.fr

ABSTRACT

The Hayabusa2 mission from the Japan Aerospace Exploration Agency (JAXA) returned to Earth samples of carbonaceous asteroid (162173) Ryugu. This mission offers a unique opportunity to investigate in the laboratory samples from a C-type asteroid, without physical or chemical alteration by the terrestrial atmosphere. Here, we report on an investigation of the mineralogy and the organo-chemistry of Hayabusa2 samples using a combination of micro- and nano- infrared spectroscopy. Particles investigated with conventional FTIR spectroscopy have spectra dominated by phyllosilicate related absorption, as observed for samples of CI-chondrites, selected ungrouped carbonaceous chondrites, and selected hydrated micrometeorites. Ryugu samples show smaller sulfates related absorption than CI-chondrites. Our samples that were only briefly exposed to the Earth atmosphere show absorptions related to molecular water, revealing fast terrestrial contamination of the spectral signature at 3-µm. Overall, our FTIR data are in agreement with other work done on Ryugu samples, revealing a low degree of mineralogical variability across Ryugu samples. AFM-IR mapping of the grains show the presence of a micrometer-sized organic globule in one of our analyzed grains. The AFM-IR spectra obtained on this globule is similar to IR spectra obtained on IOM suggesting that it is constituted of refractory organic matter. This globule may host silicate in its interior, with a different mineralogy than bulk Ryugu phyllosilicate. The shape, presence of peculiar silicate, and the nature of organic constituting the globule point toward a pre-accretionary origin of this globule and that at least part of Ryugu organics were inherited from the protosolar nebulae or the interstellar media. Altogether, our results further the similarities of Ryugu samples to CI-chondrites.

Keywords: Ryugu, Organic globule, Atomic Force Microscopy-Infrared spectroscopy (AFM-IR), NanoIR3s

INTRODUCTION

In late 2020, samples of the dark asteroid Ryugu (Cb spectral type) were returned to Earth after a >5 billions of kilometres trip made by the Hayabusa2 spacecraft, built by the Japan Aerospace Exploration Agency (JAXA). Early investigations of the samples revealed that Ryugu particles share many characteristics of chemically primitive but also highly aqueously altered CI-group of carbonaceous chondrites (Yokoyama et al., 2022; T. Nakamura et al., 2022; Noguchi et al., 2022; Yada et al., 2022). Therefore, the Hayabusa2 samples offer the unique opportunity to investigate exceptionally fresh CI material. Hayabusa2 samples were protected from interaction with the oxidizing terrestrial atmosphere from capsule recovery to curation process, and they were also protected from thermal and mechanical modification during atmospheric entry.

The relation to CI-meteorites was drawn from chemical, mineralogical and isotopic similarities (Yokoyama et al., 2022; T. Nakamura et al., 2022; Yada et al., 2022; Noguchi et al., 2022; Naraoka et al. 2023, Yabuta et al. 2023, Dartois et al. 2023). CI chondrites show an interplay of ingredients down to the sub-micrometer scale (Tomeoka and Buseck, 1988, Le Guillou et al., 2014), which requires analytical techniques with sub micrometer spatial resolution to separate their composition and understand their petrographic relations. Infrared spectroscopy (IR) is an effective method and a non-destructive technique for molecular-atomic scale vibrations of organic and inorganic compounds in extra-terrestrial materials (Kebukawa et al., 2011; Orthous-Daunay et al., 2013; Beck et al., 2014; Phan et al., 2021). However, conventional IR spectrometers use mirror-based optics to focus the beam on the sample and thus the spatial resolution is limited by diffraction. This IR diffraction limitation can be overcome by using AFM-IR (Atomic Force Microscopy-Infrared Spectroscopy), based on the combination of infrared spectroscopy and atomic force microscopy to efficiently distinguish spectral signatures of the different constituents (Dazzi & Prater, 2017; Mathurin et al., 2019). This technique has been successfully applied to extra-terrestrial materials (Mathurin et al., 2019; 2022; Kebukawa et al., 2018; Yesiltas et al., 2021; Phan et al., 2022; Noguchi et al., 2022; Yabuta et al., 2023; Dartois et al., 2023).

Here we report our work to understand the mineralogy and petrography of fine-grained Ryugu samples as part of the Preliminary Examination Team (Noguchi et al., 2023) using photothermal AFM-IR spectroscopy. Across our investigations we gained insights into the mineralogy and chemistry of phyllosilicates, and we report on the discovery of a “large” organic-dominated globule.

MATERIALS AND METHODS

Fine-grained Ryugu C0105 samples

After their arrival on Earth in December 2020, the Ryugu samples were transported from JAXA's Extraterrestrial Sample Curation Center in Sagamihara, Japan to the Mineralogy and Petrography fine-grain (Sand) initial analysis team at Kyoto University (Noguchi et al., 2023). Two grains of Ryugu from chamber C (C0105-003200401 and C0105-00380010), designated C0105-0032 and -0038 in the following text, were then sent to University Grenoble Alpes for Micro-FTIR, AFM-IR and SEM-EDS analyses.

Ryugu fragments were tightly pressed between two diamond windows (type IIa diamond, 3 mm diameter and 500 µm thick), generating to thin and flat samples (1-5 µm thick, with a typical area of 50 µm x 50 µm). One of the two windows was removed to avoid interference and to minimize beam intensity loss during transmission mode measurements. This sample preparation significantly reduced scattering artifacts and was well suited for conventional micro-FTIR. These pressed samples were also used for AFM-IR measurements. Typically, meteorite grains were prepared by crushing 10 – 20 µm fragments between two diamond windows, while the Ryugu samples were collected at around 1-5 µm. Before AFM-IR analysis, all samples were analysed using conventional micro-FTIR analysis, in order to select regions of interests (ROI).

Methods

Micro-FTIR spectroscopy

The micro-infrared spectra were measured with a Bruker Hyperion 3000 infrared microscope at the Institut de Planétologie et d'Astrophysique de Grenoble (IPAG, Grenoble, France). Spectra were measured in transmission and obtained by putting the diamond window in a custom-made environmental chamber, which expose the sample to secondary vacuum, and elevated temperature if needed (up to 300°C). This procedure enables removal of molecular water that can perturb the IR spectra in the 3-µm range (4000-3000 cm^{-1}), and also around 1630 cm^{-1}. Spectra were obtained for areas that are typically 50 µm x 50 µm.

Atomic force microscope based infrared spectroscopy (AFM-IR) measurements

AFM-IR analyses were performed on Ryugu samples after the micro-FTIR measurements. IR images and absorption spectra were acquired using a nanoIR3s^{TM} (Bruker) located at IPAG. This system includes an atomic force microscope (AFM) probe, which can

scan the sample to generate its topographical image as well as measuring IR absorption by detecting photo-thermal expansion (Dazzi & Prater, 2017). Detailed descriptions of the NanoIR3s^{TM} (Bruker) were provided in previous publications (e.g., Phan et al., 2022, 2023) together with measurement of reference materials. Briefly, the excitation laser source is a Carmina laser (from APE company) that covers a part of the mid-IR range, from 2000 to 700 cm^{-1} with its OPO/DFG (Optical Parametric Oscillator and a Difference Frequency Generation) architecture (APE GmbH, Germany), and infrared light in the 2700 – 4000 cm^{-1} wavenumber range is supplied by an optical parametric oscillator, Firefly (FF) IR laser (M squared lasers limited, Glasgow, UK). Both contact mode (CM) and tapping IR mode (TM) were used for spectroscopy and imaging measurements. The reference signal (incoming laser intensity) is recorded prior to image and/or spectra collection, and laser alignment optimization is performed before signal acquisition at different wavelengths (or wavenumbers) in the scanned range.

AFM-IR images were obtained using the APE laser in TM with a laser power of 8.81-25% of its maximum and a pulse rate at 340 -380 kHz. These analytical conditions were optimized by choosing the lowest laser power that would provide good quality spectra without affecting the sample integrity. It is well known that laser irradiation can alter the structure of macromolecular organics (in particular using highly focused beam like in Raman spectroscopy) and the analytical protocol we used has been constructed and validated in our earlier work on meteorites and coals (Phan et al., 2022; 2023). The images were collected in the range of 2000-700 cm^{-1} at infrared wavenumbers of 1720 cm^{-1}, 1600 cm^{-1}, 1450 cm^{-1} and 1000 cm^{-1}, which correspond to the carbonyl (C=O) stretching, sp^2 aromatic (C=C), methylene (CH_2) bending and/or carbonate and/or NH_4^+ bending mode, and silicate (Si-O) stretching, respectively. Images were taken through each region of interest (ROI) from each section. In addition, AFM-IR images in the range of 3800-2700 cm^{-1} were acquired using the Firefly laser in CM, which can be resolved into discrete bands including the stretching of -OH (3600 – 3700 cm^{-1}), asymmetric stretching of CH_3 (2960 cm^{-1}), asymmetric stretching of CH_2 (2930 cm^{-1}), symmetric stretching of CH_3 (2880 cm^{-1}) and symmetric stretching of CH_2 (2860 cm^{-1}) (Beck et al., 2010; Dazzi & Prater, 2017; Jubb et al., 2019; Phan et al., 2022). To better visualize the spatial distribution of different components, composite RGB color images were created by superimposing three different absorption images using the Anasys software. Before overlaying the images, each individual image was realigned to compensate for any small drifts between AFM-IR image recordings. The scan speed of all maps was 0.1 Hz and the scan sizes were from 300 × 300 to 500 × 500 points depending the size of ROI.

Local AFM-IR spectra were also obtained for two grains, C0105-0032 and C105-0038 pressed grains. For C0105-0032, the spectra were acquired in TM using the APE laser, while for C0105-0038, the spectra were acquired in CM using both the APE in the range 2000-700 cm^{-1} and the Firefly laser in the range 3800-2700 cm^{-1}. To avoid damaging the samples and obtain high-quality spectra, the incident laser power was kept to 1.22-5.03% of its maximum and the pulse rate was maintained at 240-300 kHz (Phan et al., 2022; 2023). The IR spectra were optimized at a constant laser power level for each wavenumber, with the laser power recorded with an IR sensitive photodetector. Each AFM-IR spectrum was obtained at selected points with a wavenumber spacing of 4 cm^{-1} and we have used co-averages of 3 spectra and 5 spectra for the APE and Firefly laser, respectively. For the spectral range of 2000 – 700 cm^{-1}, a gold-coated semi-tap probe (PR-EX-TnIR-A-10, 75 ± 15 kHz, 1-7 N/m) was used to avoid artifact effects due to the silicon IR absorption and allow to work both CM and TM. For the spectral range of 4000 – 2700 cm^{-1}, the images and spectra are acquired in CM with "pure contact" model PR-EX-nIR2-1, a resonant frequency of 13 ± 4 kHz and a spring constant of 0.07 – 0.4 N m^{-1}.

Scanning electron microscopy (SEM) and energy dispersive spectroscopy (EDS) measurement

After AFM-IR analysis, the samples were coated with a thin gold (Au) film for observation with a scanning electron microscope in secondary and backscattered electron modes. A JEOL JSM-7000F scanning electron microscope (SEM) equipped with an energy dispersive spectroscopy (EDS) (USA, Inc, Peabody, MA) was used at the Consortium des Moyens Technologiques Communs (CMTC, University Grenoble Alpes, France). EDS maps of carbon (C), oxygen (O), silicate (Si), aluminum (Al), iron (Fe), nickel (Ni) and sulfur (S) were collected at the acceleration voltage of 10kV and the beam current of 30 nA. EDS spectra were also collected to drive more details on the global composition of each section (Supporting Information).

RESULTS

Grain C0105-0032

Using the tapping IR mode (TM), we studied the spatial distribution of organic and mineral infrared signatures throughout the entire surface of the C0105-0032 and C0105-0038. A 5 µm × 5 µm ROI of C0105-0032 was analyzed with a higher spatial resolution of 500 × 500

points (e.g., spatial resolution imaging of ~ 10 nm) (Fig. 1A). AFM-IR images obtained at different wavelengths show the distribution of different vibrational bonds: carbonyl (C=O) (in red, at 1720 cm^{-1}), aromatic (C=C) (in pink, at 1600 cm^{-1}), carbonate (CO_3) or CH_2 bending mode groups (in blue at 1450 cm^{-1}), sulfate (SO_4) (in yellow, at 1100 cm^{-1}), and phyllosilicate (Si-O) (in green, at 1000 cm^{-1}) (Fig. 1B-F). Figure 2B-C shows a color composite RGB map (1720, 1600 and 1450 cm^{-1} IR intensity) and individual absorption map at 1450, 1100 and 1000 cm^{-1}, together with the locations where full spectra were collected in the 2000 – 700 cm^{-1} range.

These maps enable to identify different domains (Fig. 1-2). Overall, the most widespread absorption is the band at around 1000 cm^{-1}, which can be attributed to Si-O stretching in phyllosilicates (green area in Fig. 2B and 2C). This observation agrees with the fact that Ryugu fine-grained samples mineralogy is dominated by phyllosilicates (Noguchi et al., this volume). Isolated blue and violet (Fig. 2B and 2C) areas are also observed in the RGB maps, and are interpreted to be micro to sub-µm sized carbonate grains.

Only a few areas are red in Fig 2A can be explained by pure organics. The map obtained at 1720 cm^{-1}, intended to probe the C=O mode, shows a strong correlation to carbonates signatures. Several areas appear yellow in Fig. 2C, meaning that they display particularly strong signatures around 1100 cm^{-1}, which may be interpreted by the presence of sulfate.

In order to gain further insights in the constituents of our Ryugu grains we collected an array of more than 100 single-point AFM-IR spectra in the 2000 – 700 cm^{-1} range (in tapping IR mode), that can be compared to µ-FTIR spectra of the grains as well as to reference spectra of possible mineral components (e.g., saponite, dolomite, calcite) and the Orgueil CI chondrite (Phan et al., in prep) (Fig. 2D). We averaged 90 spectra, exhibiting a similar signature (P spectra in Fig. 2D) and compared them to 13 different spectra obtained at locations marked P1-P10 and C1-C3. The average spectra (P) in the green region have a strong and narrow absorption at 1000 cm^{-1}, similar to FTIR spectra observations, which are attributed to phyllosilicate (Si-O), and the best spectral analogue to date is a saponite spectra (Beck et al., 2014), with possible contribution from serpentine (Dartois et al., 2023).

The C2 and C3 spectra also display strong absorption at 1440 cm^{-1} and 880 cm^{-1} band attributed to carbonate (Fig. 2D). Carbonates were found in mm-sized grains (Nakamura et al., 2023) and smaller isolated or aggregated grains (Yabuta et al., 2023; Dartois et al., 2023) of a few to ~ 30 µm size. Dolomite is the dominant carbonate in the Ryugu coarse samples (1-8 mm) which were formed by aqueous alteration reactions at low temperature, high pH and water/rock

ratios <1 (Nakamura et al., 2023). Porous dolomite and magnetite that occur in some frothy layer are thought have been modified by space weathering processes (Noguchi et al., 2023).

Interestingly, spectrum C1 in the redder location in Fig. 2B reveals faint but distinct peaks at 1720 and 1600 cm^{-1} attributed to C=O and C=C present together with the strong peak at 1000 cm^{-1} implying the presence of organic matter associated with Mg-rich phyllosilicate (Fig. 2D). A diffuse organic component within the phyllosilicate matrix may be present in the grain, but in tapping IR mode, these faint organic signatures are generally absent from the AFM-IR spectra (Fig. 2D-E) (Phan et al., 2022; 2023). In addition, spectra obtained at the P1- P10 that have different absorption at 1100 and 860 cm^{-1}, probably due to different types of sulfate and/or silicate (Madejová et al., 2017) (Fig. 2E).

Grain C0105-0038

The grain of C0105-0038 (Fig. 3A) was fractured into several smaller grains, then crushed between two diamond windows (Fig. 3B), and the micro-FTIR spectra measured are displayed in Fig. 3C. The Ryugu bulk samples infrared transmission we obtained appear similar to those measured for CI chondrites such as Orgueil or Ivuna (Nakamura et al., 2023; Yokoyama et al., 2022). A band at 3690 cm^{-1} is observed, corresponding to an -OH stretching mode in a Mg-rich phyllosilicate. This band is weak in Fig. 3C since the pressed sample was particularly thin. In the 3000 – 2800 cm^{-1} range several bands are observed with peaks at 2952, 2925, 2873 and 2857 cm^{-1}. These peaks are attributed to the asymmetric and symmetric stretching modes of the CH_3, CH_2 and CH groups, related to complex interactions between overtones and fundamental vibrations. Spectra obtained in all sections reveal the presence of a sharp feature at 1000 cm^{-1} that can be attributed to phyllosilicate. Unlike the other samples, grain 4 (G4) presents a strong signature at 1440 and 880 cm^{-1} that can be attributed to carbonate bending and in-plane mode, respectively (Phan et al., 2022).

A 20 × 20 μm^2 area of grain 3 (G3) (red spectra in Fig. 3) was imaged in AFM-IR tapping mode (Fig. 4). Different from C0105-0032 grain, this grain does not display a signature around 1100 cm^{-1}, meaning that sulfate is absent. Similarly, AFM-IR intensity was measured at 1720, 1450 and 1000 cm^{-1}, corresponding to carbonyl (C=O), carbonate (CO_3) and phyllosilicate (Si-O) (Fig. 4C-E). These maps and the associated RGB composite map we produced (Fig. 4F) show an intense signal at 1000 cm^{-1} throughout the sample (green) that can be attributed to phyllosilicate. This map also shows grains with strong AFM-IR intensity in all three

wavelengths (bright green in the RGB composite), that are interpreted to be phases with high refractive index (Fe-oxides, metal and sulfides) which was confirmed by SEM imaging and is corroborated by other studies (Dartois et al., 2023). Several small grains appear in blue in this map, and are interpreted to be small carbonate grains.

Interestingly, a small circular area in the right bottom corner of the map shows a strong signature at 1720 cm^{-1} (Fig. 4C and 4F) corresponding to C=O in organic matter. An array of 50 spectra was collected in the green zone (Si-O array) and one spectrum (A1) was obtained on the "red globule" in the RGB composite map (Fig. 4B and 4F). In addition to the organic globule, organic signatures are present as a diffuse component within the phyllosilicate (Average Si-O spectra), as evidenced from the presence of aromatic (C=C) band at 1600 cm^{-1} (Fig. 4G) and a small feature around 1720 cm^{-1}. In the average spectra of "green" areas, a broad band around 1000 cm^{-1} is present, similar to results obtained from grain C0105-0032, and attributed to Si-O in phyllosilicates. Note that in the phyllosilicate-rich areas, the water bending mode at 1630 cm^{-1} can contribute to some extent to this spectral region. While Ryugu grains analyzed following an air-shutoff procedure do not show strong evidence for molecular water (Nakamura et al., 2023), our samples that were exposed to air probably experienced re-hydration to some extent.

The A1 spectrum obtained on the red globule shows three distinct peaks at 1720, 1600 cm^{-1} and 1450 cm^{-1} attributed to the C=O, C=C and CH_2 bending mode in organic matter (Fig. 4G). This spectrum is reminiscent of infrared spectra obtained on insoluble organic matter (Orthous-Daunay et al., 2013; Quirico et al., this volume), or organic particle found in Orgueil (Phan et al., 2022) (Fig. 4G).

Comparison to µ-FTIR spectra obtained on the same grain, reveals a good consistency between local AFM-IR and conventional µ-FTIR spectra (Fig. 4G). The µ-FTIR spectra (in black) can be well explained by a mixture of average AFM-IR phyllosilicate spectra, and carbonates (to explain the 1450 cm^{-1} slightly more elevated in the FTIR spectrum of the grain than in the average AFM-IR spectrum of phyllosilicates) and the different probe depths of the two techniques.

While no phyllosilicate signal was detected in the globule area, the AFM-IR spectra reveal a broad absorption massif with a maximum around 1050 cm^{-1}. The fact that no signal was detected in the AFM-IR map is related to the fact that AFM-IR maps are obtained in tapping mode, more sensitive to the surface, while AFM-IR spectra are obtained in contact mode, that probes a larger volume of sample. The different shape of the 1000-1050 cm^{-1} band between the

organic globule and typical Ryugu phyllosilicate is related to the presence of a different type of silicate (amorphous?) or contribution from organic vibration to this spectral region.

To further elucidate the mineralogy and structure of the organic matter in this area, we collected AFM-IR maps of a 3 × 3 μm^2 area (Fig. 5A) around the organic globule at wavelengths similar to those used for the larger area (1720, 1600, 1450, and 1000 cm^{-1} shown in Fig. 5B-E). As can be seen in Fig. 5F, this region shows a significant contribution from the Si-O stretching of the phyllosilicates in the 1000 cm^{-1} map, but these contributions are absent in the central organic-rich area. Conversely, the central part corresponding to the organic globule shows a strong 1720 cm^{-1} absorption related to C=O. The region also shows infrared absorptions at 1600 cm^{-1}, 1450 cm^{-1} as shown in Fig. 5C-D, which are spatially correlated and can be attributed to aromatic (C=C) or/and water molecules, and aliphatic organic compounds, respectively. In addition, the IR maps also show areas with strong and correlated intensity at 1600 cm^{-1}, 1450 cm^{-1}, and 1000 cm^{-1}, which may reveal the presence of high refractive index Fe-bearing minerals such as Fe sulfide and Fe-Ni sulfides (Dartois et al., 2023), as shown in the Fe, Ni, S, and BSE EDS images obtained after the AFM-IR measurement (Fig. S-1 and S-2).

The micro-globule apparent in the 1720 cm^{-1} absorption image, is circular, and has a diameter of ~ 1 μm (Fig. 5F). This globule was further investigated with full AFM-IR spectra (Fig. 6) at the locations indicated in the AFM composite images (Fig. 6A-B). The first spectrum at the central globule location (A1) reveals two distinct peaks and shows a higher aromatic peak intensity (C=C) at 1600 cm^{-1} and less carbonyl (C=O) at 1720 cm^{-1} than in the bulk organic particles we analyzed in Orgueil (Fig. 6C) (Phan et al., 2022). The weak peak at 1450 cm^{-1} is attributed to the CH_2 bending mode, carbonate or NH_4^+ bending mode, which are all in this spectral area. Although the sample IR images show no signal at 1000 cm^{-1} (Fig. 5E), the contact IR spectrum reveals a prominent peak at 1050 cm^{-1} that has moved from the phyllosilicate position at 1000 cm^{-1} (Fig. 4G and Fig. 6C-D), following results obtained in our first investigations of the globule.

A series of spectra were collected in the globule from the center outward (labeled A1-A8 and B1-B8) in positions shown in the AFM and RGB images (Fig. 6 A-B) to better understand the variation of the organic and silicate structure inside and outside the organic globule. The spectra obtained are consistent with the presence of macromolecular organics as part of the globule. As can be seen, the CH_2 and CH_3 bending modes (1450 and 1380 cm^{-1}) or the broad congested band ~1250 cm^{-1} (C-O, C-C, OH, etc.) appear in all spectra within the globule (e.g., A1-A6 and B1-B4) and are consistent with observation of IOM in chondrites using

conventional μ-FTIR spectroscopy (Kebukawa et al., 2011; Orthous-Daunay et al., 2013). In these spectra we also confirm the presence of the broad absorption massif with a maximum around 1050 cm^{-1}. Looking at the relative intensity of the C=O and C=C modes, the organic structure appears to be increasingly less aromatic while the silicate peak shape becomes thinner from the center outward (Fig. 6C-D).

DISCUSSION

Infrared mineralogy and comparison with other extra-terrestrial materials

The silicate mineralogy of Ryugu fine-grained samples is dominating by a mixture of "coarse"- and "fine"- grained phyllosilicates, with chemical compositions intermediate between saponite and serpentine (Noguchi et al., this volume). The presence of saponite and serpentine domains was confirmed by High-Resolution bright field TEM (Noguchi et al., this volume). Serpentine and saponite are expected to have different mid-infrared spectra in the 10-μm range where Si-O stretching occurs, at least in the case of well-crystallized serpentines (Beck et al., 2014, Dartois et al., 2023). Interestingly, the serpentine-rich CM chondrites like ALH 83100 have infrared spectra in the 10-μm range clearly distinct from CI-chondrites (Fig. 7), meaning that even low-crystallinity serpentines, generally dominate the mineralogical composition in CM chondrites, can be distinguished from saponite; accordingly, a band is more in line with serpentine measurement. Based on IR, the mineralogy of our Ryugu "sands" seem related to saponite, rather than serpentine or a mixture of both.

Ryugu samples from the IOM and stone team were investigated with similar techniques by Dartois et al. (2023). In their work, the spectral range covered is similar to that in our study, (slightly broader in Dartois et al. (2023) as it goes down to 100 cm^{-1}). A difference between these two works is that, in our case, FTIR measurements were done in a custom-made environmental cell enabling exposure of the sample to vacuum and gentle heating (80°C). This procedure enables to remove weakly bonded water molecules. Overall, the FTIR spectra we obtained on fine-grained samples from the sand-team are highly similar to those obtained by Dartois et al. (2023), and the AFM-IR images and spectra obtained in both works are in agreement. Therefore, the combination of our work and Dartois et al. (2023) reveals a certain homogeneity of Ryugu mineralogy over a range of grain sizes.

Spectra of CI chondrites show a shoulder around 1200 cm^{-1} that can be related to the presence of sulfates, and this shoulder is absent from Ryugu samples. At least a fraction of sulfates minerals in CI chondrites are interpreted to be of terrestrial origin (Gounelle &

Zolensky, 2001, 2014; Nakamura et al., 2023; Viennet et al., 2023) and samples from Ryugu are fresher in that sense. Still, we observed that one of the samples studied shows signature of small sulfate grains (<1 µm) than can be interpreted as products from the fast terrestrial oxidation of iron sulfides. The signatures of carbonates at 880 and 1450 cm^{-1} present in the spectra of the ungrouped carbonaceous chondrites Tarda and Tagish Lake (Fig. 7), are absent in the spectra of the Ryugu grain shown in Figure 7, but carbonates were identified with AFM-IR and in other grains with µ-FTIR analyses.

Overall, from an infrared point of view, the clay mineralogy of Ryugu is similar to other CI chondrites, some lithologies of Tagish Lake, and some other samples belonging to the magnetite- and ^{17}O-rich group of carbonaceous chondrites (Fig. 7, Hewins et al., 2021). It is interesting to note that these meteorites, in addition to having some commonalities from a chemical point of view, also present some similarities in the clay mineralogy. We also present in Figure 7, a typical spectrum obtained on a fine-grained hydrated micrometeorite from (Battandier et al., 2018). We can observe in this graph that hydrated micrometeorites are similar to Ryugu samples and CI chondrites, and clearly distinct from CM chondrites (Fig. 7). The similarities between Ryugu, CI chondrites, hydrated IDPs and micrometeorites are also discussed in Noguchi et al. (this issue).

An organic micro-globule

While organic globules had been observed in different types of meteorites (e.g. Claus and Nagy, 1961; Alexander et al., 2017), the discovery of an organic globule analyzed *in situ* (without liquid or acid extraction) and on a fresh meteorite fall (Tagish Lake) provided clear and non-ambiguous evidence for an extra-terrestrial origin of at least some of the globules (Nakamura et al, 2002). While these structures are often referred to as “nano”-globules, their size range goes up to more than a micrometer in diameter (140-1700 nm in Nakamura et al., 2002; 150 nm to 1150 nm in De Gregorio et al., 2013). We will refer here to the term globule to describe a spherical organic grain (>100 nm), that may contain a mineral grain in its interior (and in that case it is equivalent to a spherical coating). The globules can be solid or hollow, and may present some layering in their interior (Vollmer et al., 2020a). They are made of H, O and N bearing organic carbon and can be host to isotopic enrichment for C, N or H, but not systematically and variably (Nakamura-Messenger et al., 2006; De Gregorio et al., 2013; Vollmer et al., 2020b). For example, some nanoglobules from ALH 77307, Murchison and Orgueil were not isotopically enriched (De Gregorio et al., 2013). They were also found to have

different organo-chemistry, with some globules enriched in aromatic moieties, while others having a composition more similar to insoluble organic matter (IOM) (De Gregorio et al., 2013). In the case of Ryugu sample, a carbon nano-globule was observed by Ito et al. (2022), which was hosting a silicate phase in its interior. Hollow and solid nanoglobules have also been observed in IOM samples extracted from Ryugu grains, and showing both aromatic-rich and IOM compositions (Yabuta et al., 2023).

Physical properties of this "lentil" globule

The AFM-IR probe configuration in our measurements is not able to distinguish whether the globule we observed is solid or hollow (Fig. 5F). We note, however, that based on the combined 3D view of AFM topography and RGB composite maps, the globule is not flat or spherical but "lentil" shaped (Fig. 5F). The AFM topographical image shows its apparent diameter is around 1-µm, while the physical height of the shape protruding from Ryugu phyllosilicates matrix is only around 100 nm. This "lentil" shape could be related to sample preparation, but we would rather expect a flat surface in that case. This shape may represent the original structure of the globule, but most of it is buried in the surrounding matrix. An alternative possibility is that the globule was hollow, with a spherical shape and collapsed at some point.

After our investigations on the globule in the 7-13 µm range with the APE laser source, we attempted to characterize its aliphatic linkage using the Firefly laser source (2.5-4 µm). For hardware reason, chemical mapping using this laser source was only possible using AFM contact mode, and not tapping mode like for the APE source. This mapping led to the disruption of the globule and the organics that were constituting the globule were somehow spread over the surface (See SI, Fig. S-3 and S-4). We also note that the areas for which APE spectra were collected (in contact mode) are visible in the AFM-IR map obtained after spectral measurements (Fig. 5B). The three small pits are due to the indentation of the globule by the AFM-tip. This attests that the globule is somehow weak in physical nature.

The nature of organic matter in fine-grained samples and in the globule

Organic compounds were investigated by several techniques in Ryugu samples and revealed a direct link between macromolecular organic matter in C-type asteroids and that in primitive carbonaceous chondrites. Basically, four main chemical forms of carbon have been observed in Ryugu grains as diffuse, highly aromatic, aromatic and IOM-like organic matter.

Particles and globules tend to show more highly carbonyl and aromatic compositions, while diffuse organics more dispersed throughout the sample resemble IOM-like organic matter (Yabuta et al., 2023, Rhonda et al., this volume). In the present study, both organic globule and diffuse organics in fine-grained Ryugu were observed by AFM-IR measurements. The spectral range covered by the APE laser can in principle be used to obtain information on the aromaticity of the organic compounds, provided that the contribution of carbonates to the 1450 cm^{-1} feature (CH_2 group) is negligible. In that case, the ratio of the 1450 and 1650 cm^{-1} (aromatic C=C) band can be used as a semi-quantitative tracer of aromaticity. Nevertheless, molecular water in the phyllosilicate may lead to a spectral superposition between the organic C=C and C=O bands and the water bending mode around 1630 cm^{-1}, which can be removed by heating the sample in vacuum with conventional µ-FTIR (Beck et al., 2010; Orthous-Daunay et al., 2013) but cannot be removed with our AFM-IR setup.

In the case of two C0105 grains, diffuse organics seem to be present based on the AFM-IR maps but the spectral range where the doublet of bands at 1720 and 1600 cm^{-1} occurs (attributed to C=O and C=C) is perturbated by the water bending mode. The intensity ratio of C=O and C=C is significantly lower than that of Ryugu IOM from µ-FTIR spectra (Quirico et al., this volume) (Fig. 8), suggesting a contribution of water to the C=C position near 1600 cm^{-1} or that diffuse organics are less carbonylated than IOM. Peak fitting by Dartois et al. (2023) to disentangle between molecular water and C=C signatures seems to show that at least some grains have a contribution from aromatic-rich organics in this spectral range.

Aliphatic organics are present in Ryugu fine-grained samples as evidenced by the modes around 3.4-3.4 µm seen in our conventional µ-FTIR spectra, which cannot be due to globules given their rarity, and which has been observed through STEM-EELS-EDS (Yabuta et al., 2023). This diffuse aliphatic organic fraction is similar to that of Orgueil (Guillou & Brearley, 2014; Phan et al., 2022). It has been suggested that some of these compounds may be hosted within the interlayer space of phyllosilicates (Viennet et al., 2023). The comparison between spectra of intact Ryugu grains and IOM show that the CH_2/CH_3 ratio, determined from the ratio of the antisymmetric stretching modes of the CH_2 and CH_3 chemical groups is higher for intact grains compared to IOM (Dartois et al., 2023; Quirico et al., this volume) (Fig. S-4). This supports the view that diffuse organic matter is a mix between IOM and soluble organic molecules that are lost during the chemical extraction of IOM.

The AFM-IR spectra obtained on the globule are presented in Figure 6, while some structural parameters (C=O/C=CC and CH_{2bend}/C=C) derived from these spectra are shown in

Figure 8A-B. At first glance, the spectra obtained on the globule are reminiscent of measurements obtained on IOM samples (Quirico et al., this volume). A difference is the presence of a broad absorption at 1050 cm^{-1} that we attribute to silicates under or inside the globule (see discussion below). Some spectral variations were found inside the globule, with an increase of the C=O/ C=C and CH_{2bend}/C=C from the center to the exterior (Fig. 8) of the globule. Overall these parameters are in line with values obtained for Ryugu's IOM (Fig. 8), revealing that the organic chemistry of the globule is similar to IOM.

The IOM PET team analyzed in detail the organo-chemistry of refractory organics from Ryugu samples, as well as their isotopic composition (Yabuta et al., 2023). Organic globules were found and investigated by several techniques revealing the presence of both IOM-like and aromatic globules, with grain size ranging typically 50-500 nm up to 2000 nm in diameter. The globule we investigated here is therefore amongst the largest ones found in Ryugu so far. Both IOM-like and aromatic globules were found in Yabuta et al. (2023), while the only globule we detected is IOM-like. However, aromatic globules may be more difficult to detect with AFM-IR due to the interference with molecular water, and the lack of 1720 cm^{-1} peak.

Silicates inside the globule?

The organic globule identified by Ito et al. (2022) in Ryugu samples revealed the presence of a silicate particle in its interior. A carbon globule with a silicate core was also observed in the CR2 chondrite NWA 801 (Hashiguchi et al., 2013) and in Renazzo-type CR chondrites GRA 95229 (Vollmer et al., 2020a). In our case, while the AFM-IR maps obtained in tapping mode revealed the absence of signal in the Si-O region in the globule, contact mode spectra showed the presence of a broad band around 1050 cm^{-1}, probably due to silicate signature for AFM-IR spectra obtained within the globule. Contact mode AFM-IR spectra may probe a larger volume around several micrometers under the surface (Mathurin et al., 2022), and may be picking signals from below or inside the globule. Given the diameter of the globule and the spatial resolution of contact mode IR spectra (Phan et al., 2022), it is unlikely that this silicate signature comes from the phyllosilicates on the side of the globule. It can also be noted that this silicate signature is distinct from typical phyllosilicates signatures obtained from Ryugu samples, with a broader shape and maxima of absorption around 1050 cm^{-1}. The spectra obtained on the globule also show a feature around 800 cm^{-1}, not seen in other spectra obtained on Ryugu. This band could be related to Si-O-Si bending in SiO_2, or to Fe^{3+}-OH in a phyllosilicate (Madejová et al., 2017). The fact that this silicate signature is particular, and was

found only associated to the globule may suggest that this phase may be located inside the globule. However, this argument remains circumstantial at best without excavation and direct observation of the grain interior.

Possible formation mechanisms

We typically surveyed an area of more than 2500 μm^2 fine-grained Ryugu samples with AFM-IR, while the surface of the nanoglobule is of less than 1 μm^2. Therefore, carbon-rich globules are rare and the amount of C present in the form of globules is likely insufficient to be the dominant reservoir of carbon in Ryugu samples, since the bulk organic C content is of about 3 wt.% (Yokoyama et al., 2022). Several possible formation mechanisms and formation environments have been proposed for the carbon-rich globules encountered in carbonaceous chondrites. They were summarized in the thorough investigation by De Gregorio et al. (2013). The possible formation environments includes pre-solar, solar nebula or asteroidal. If pre-solar, these globules may be inherited directly from the diffuse interstellar medium (DISM), where carbonaceous compounds could form a shell surrounding an ice-silicate core (Greenberg et al., 1995). In the solar nebula scenario, carbon globules may be the leftover of gas-phase or solid-state chemistry in the solar parent molecular cloud or the protosolar nebula. Globular-shape carbon-rich particle have been produced experimentally by two-step UV-irradiation of ice-mixture (Piani et al., 2017) or warm plasma chemistry (Bekaert et al., 2018). However, the capability of such mechanism to reproduce the peculiar structure of IOM remains to be assessed (Quirico et al., 2020). A last formation environment that has been proposed for carbon-rich globules is on the parent planetesimal, where their formation would be triggered by the presence of liquid water on these objects. In the study of Cody et al. (2011), micrometer-sized globule with morphologies reminiscent of meteorite observations were produced from the liquid-phase polymerization of formaldehyde. Another possibility is that the presence of liquid water on the asteroid could have induced mobilization of a diffuse organic fraction, and led to their condensation locally. In that sense, the organic-globule would form as coatings surrounding a pre-existing grain such as discussed by (Vollmer et al., 2020a).

In our study, only one globule was observed, but for the first time we were able to extract the IR spectra of a single globule, *in situ*. Our observation reveals strong similarities with insoluble organic matter, and that this globule in not particularly enriched in aromatic moieties. This IOM-like chemistry is consistent with analyses on IOM extracted from the CI Orgueil by De Gregorio et al. (2013), for which no aromatic globule was found unlike CR chondrites for

instance. In our work, we observed some chemical variability within the globule based on the C=O/C=C ratio, where the outer part of the globule appears enriched in C=O. This may record the history of the globule synthesis, or its chemical modification upon hydrothermal alteration.

The fact that the globule seems to be associated to a silicate phase distinct from the typical phyllosilicates from Ryugu, as observed in Ito et al. (2022) and our study, suggests that the globule was not produced on the asteroid; in the parent body mechanisms suggested in the above paragraph, none would lead to preferential formation of the globule around a specific type of silicates. One possibility is that the migration and coalescence of organic-compounds occurred at the very beginning of the aqueous alteration process, and the presence of the coating protected the silicate from conversion to phyllosilicates. While parent-body formation cannot be strictly excluded, our preferred explanation is a pre-accretionary origin, but the exact environment and synthesis mechanism remain elusive. The oxygen isotope of the silicates associated to the carbon globule in the CR2 chondrite NWA 801 were measured by Hashiguchi et al. (2013). Their results showed that oxygen isotopes in the silicate are similar to solar system material, suggesting then a solar system origin for the globule. Similar work done on Hayabusa2 samples may help understand the formation environment of the carbon globules from Ryugu.

CONCLUSION

Here, we report on an infrared spectroscopy study of fine-grained particles from the Ryugu asteroid, as part of the Hayabusa2 PET "sand" team. Infrared absorption properties were obtained on grains at the 100 µm x100 µm scale using conventional FTIR, and at the sub-µm scale using photo-thermal AFM-IR.

This works confirms that the mineralogy of Ryugu fine-grained material is dominated by phyllosilicates. These phyllosilicates are Mg-rich and have infrared properties similar to saponite, based on the 10-µm silicate absorption feature. They are clearly distinct from CM chondrites, and similar to observations on other CI chondrites or selected ungrouped carbonaceous chondrites, as well as to some hydrated micrometeorites. The sulfate signature seen in CI chondrites are absent from our FTIR spectra of Ryugu samples. We also observe carbonate ion signatures in the transmission FTIR spectra, and these ions are expected to be present in a dolomite crystallographic structure.

Further investigations of the Ryugu "sands" mineralogy and organic compounds was performed using AFM-IR, enabling to probe the sub-µm scale. We observe little variability of

627 the Si-O stretching, showing a relative homogeneity of the phyllosilicate from an IR perspective
628 at that scale. We observe the presence of small carbonate grains (100-500 nm) finely mixed with
629 the phyllosilicate. In one of the studied areas, small particles associated to a band at 1100 cm^{-1}
630 are present and interpreted to be terrestrial sulphate forming at the expense of S-bearing
631 opaques.

632 Analysis of organic signatures reveals the presence of a diffuse organic component, from
633 the presence of CH-modes, and we observe a single carbon-rich globule from AFM-IR mapping.
634 This globule is roughly 1-µm in diameter and AFM-IR spectra obtained revealed the presence
635 of C=O and C=C, and CH_2-bend, in a similar way to IOM extracted from Ryugu samples. From
636 our study, carbon globule is rare in Ryugu and likely represent only a fraction of the carbon
637 budget in Ryugu; but detection biases may be present and inherent to our technique and sample
638 preparation protocol. This globule seems to be associated to silicate whose nature is different
639 from the typical Ryugu phyllosilicate. The presence of IOM like globules in Orgueil was
640 observed by De Gregorio et al. (2013) after acid-leaching. Our in-situ AFM-IR analysis reveal
641 the existence of such globule in a CI-related object. A pre-accretion scenario is favored for the
642 formation of this globule, but the exact formation environment, and mechanisms, remain
643 elusive.

644

645 **ACKNOWLEDGEMENTS**

646 The Hayabusa2 project has been developed and led by JAXA in collaboration with Deutsches
647 Zentrum für Luft- und Raumfahrt (DLR) and Centre national d'études spatiales (CNES), and
648 supported by NASA and Australian Space Agency (ASA). We thank all of the members of the
649 Hayabusa2 project for their technical and scientific contributions. This research was supported
650 by the H2020 European Research Council (ERC) (SOLARYS ERC-CoG2017_771691) and the
651 Programme National de Planétologie (PNP) as well as the Centre national d'études spatiales
652 (CNES) within the framework of the Hayabusa 2 and MMX missions. We also acknowledge
653 Frédéric Charlot for the assistance during SEM/EDS analysis at CMTC (Grenoble, France).

654 **Supplementary materials**

655 Supplementary data related to this article can be found in the Supporting materials part.

656

657 *Data Availability* – The data that support the findings of this study are available from the
658 corresponding author upon reasonable request.

Reference

Alexander, C. M. O. D., Cody, G. D., De Gregorio, B. T., Nittler, L. R., & Stroud, R. M. (2017). The nature, origin and modification of insoluble organic matter in chondrites, the major source of Earth's C and N. Chemie Der Erde, 77(2), 227–256. https://doi.org/10.1016/j.chemer.2017.01.007

Alexander, C. M. O. D., Cody, G. D., De Gregorio, B. T., Nittler, L. R., & Stroud, R. M. (2017). The nature, origin and modification of insoluble organic matter in chondrites, the major source of Earth's C and N. *Chemie Der Erde*, *77*(2), 227–256. https://doi.org/10.1016/j.chemer.2017.01.007

Battandier, M., Bonal, L., Quirico, E., Beck, P., Engrand, C., Duprat, J., & Dartois, E. (2018). Characterization of the organic matter and hydration state of Antarctic micrometeorites: A reservoir distinct from carbonaceous chondrites. *Icarus*, *306*, 74–93. https://doi.org/10.1016/j.icarus.2018.02.002

Beck, P., Garenne, A., Quirico, E., Bonal, L., Montes-hernandez, G., Moynier, F., & Schmitt, B. (2014). Transmission infrared spectra (2–25 μm) of carbonaceous chondrites (CI, CM, CV–CK, CR, C2 ungrouped): Mineralogy, water, and asteroidal processes. *Icarus*, *229*, 263–277. https://doi.org/10.1016/j.icarus.2013.10.019

Beck, P., Quirico, E., Montes-Hernandez, G., Bonal, L., Bollard, J., Orthous-Daunay, F. R., Howard, K.T., Schmitt, B., Brissaud, O., Deschamps, F., Wunder, B., Guillot, S. (2010). Hydrous mineralogy of CM and CI chondrites from infrared spectroscopy and their relationship with low albedo asteroids. Geochimica et Cosmochimica Acta, 74(16), 4881–4892. https://doi.org/10.1016/j.gca.2010.05.020

Bekaert, D. V., Derenne, S., Tissandier, L., Marrocchi, Y., Charnoz, S., Anquetil, C., & Marty, B. (2018). High-temperature Ionization-induced Synthesis of Biologically Relevant Molecules in the Protosolar Nebula. *The Astrophysical Journal*, *859*(2), 142. https://doi.org/10.3847/1538-4357/aabe7a

Claus, G., & Nagy, B. (1961). A Microbiological Examination of Some Carbonaceous Chondrites. *Nature*, *192*(4803), 594–596. https://doi.org/10.1038/192594a0

Cody, G. D., Heying, E., Alexander, C. M. O., Nittler, L. R., Kilcoyne, A. L. D., Sandford, S. A., & Stroud, R. M. (2011). Establishing a molecular relationship between chondritic and cometary organic solids. *Proceedings of the National Academy of Sciences*, *108*(48), 19171–19176. https://doi.org/10.1073/pnas.1015913108.

Dartois, E., Geballe, T. R., Pino, T., Cao, A.-T., Jones, A., Deboffle, D., … D'Hendecourt, L. (2007). IRAS 08572+3915: Constraining the aromatic versus aliphatic content of interstellar HACs. *Astronomy & Astrophysics*, *463*, 635–640. https://doi.org/10.1051/0004-6361

Dartois, Emmanuel, Kebukawa, Y., Yabuta, H., Mathurin, J., Engrand, C., Duprat, J., Bejach, L., Dazzi, A., Deniset-Besseau, A., Bonal L., Quirico, E., Sandt, C., Borondics, F., Barosch, J., Cody, G. D., De Gregorio, B., Hashiguchi, M., Kilcoyne, D. A. L., Komatsu, M., Martins, Z., Matsumoto, M., Montagnac, G., Mostefaoui, S., Nittler, L. R., Ohigashi, T., Okumura, T., Remusat, L., Sandford, S., Shigenaka, M., Stroud, R., Suga, H., Takahashi, Y., Takeichi, Y., Tamenori, Y., Verdier-Paoletti, M., Yamashita, S., Nakamura, T., Morita, T., Kikuiri, M., Amano, K., Kagawa, E., Noguchi, T., Naraoka, H., Okazaki, R., Sakamoto, K., Yurimoto, H., Abe, M., Kamide, K., Miyazaki, A., Nakato, A., Nakazawa, S., Nishimura, M., Okada, T., Saiki, T., Tachibana, S., Tanaka, S., Terui, F., Tsuda, Y., Usui, T., Watanabe, S., Yada, T., Yogata, K., Yoshikawa, M. (2023). Chemical composition of carbonaceous asteroid Ryugu from synchrotron spectroscopy in the mid- to far-infrared of. Astronomy & Astrophysics, 671, 1–30.

Dazzi, A., & Prater, C. B. (2017). AFM-IR: Technology and Applications in Nanoscale Infrared Spectroscopy and Chemical Imaging. *Chemical Review*, *117*(7), 5146–5173. https://doi.org/10.1021/acs.chemrev.6b00448

De Gregorio, B. T., Stroud, R. M., Nittler, L. R., Alexander, C. M. O. D., Bassim, N. D., Cody, G. D., KilCoyne A. L. D., Sandford S. A., Milam S. N., Nuevo M., Zega, T. J. (2013). Isotopic and chemical variation of organic nanoglobules in primitive meteorites. Meteoritics and Planetary Science, 48(5), 904–928. https://doi.org/10.1111/maps.12109

Gounelle, M., & Zolensky, M. E. (2001). A terrestrial origin for sulfate veins in CI1 chondrites. *Meteoritics and Planetary Science*, *36*(10), 1321–1329. https://doi.org/10.1111/j.1945-5100.2001.tb01827.x

Gounelle, M., & Zolensky, M. E. (2014). The Orgueil meteorite: 150 years of history. *Meteoritics and Planetary Science*, *49*(10), 1769–1794. https://doi.org/10.1111/maps.12351

Greenberg, J. M., Li, A., Mendoza-Gómez, C. X., Schutte, W. A., Gerakines, P. A., & de Groot, M. (1995). Approaching the Interstellar Grain Organic Refractory Component. *The Astrophysical Journal*, *455*(2), 177–180. https://doi.org/10.1086/309834

Guillou, C. Le, & Brearley, A. (2014). Relationships between organics, water and early stages of aqueous alteration in the pristine CR3.0 chondrite MET 00426. *Geochimica et Cosmochimica Acta*, *131*, 344–367. https://doi.org/10.1016/j.gca.2013.10.024

Hashiguchi, M., Kobayashi, S., & Yurimoto, H. (2013). In situ observation of D-rich carbonaceous globules embedded in NWA 801 CR2 chondrite. *Geochimica et Cosmochimica Acta*, *122*, 306–323. https://doi.org/10.1016/j.gca.2013.08.007

Hewins, R. H., Zanetta, P. M., Zanda, B., Le Guillou, C., Gattacceca, J., Sognzoni, C., … Borondics, F. (2021). NORTHWEST AFRICA (NWA) 12563 and ungrouped C2 chondrites: Alteration styles and relationships to asteroids. Geochimica et Cosmochimica Acta, 311, 238–273. https://doi.org/10.1016/j.gca.2021.06.035

Ito M., Tomioka N., Uesugi M., Yamaguchi A., Shirai N., Ohigashi T., Liu M.-C., Greenwood

736 R. C., Kimura M., Imae N., Uesugi K., Nakato A., Yogata K., Yuzawa H., Kodama Y.,
737 Tsuchiyama A., Yasutake M., Findlay R., Franchi I. A., Malley J. A., McCain K. A.,
738 Matsuda N., McKeegan K. D., Hirahara K., Takeuchi A., Sekimoto S., Sakurai I., Okada
739 I., Karouji Y., Arakawa M., Fujii A., Fujimoto M., Hayakawa M., Hirata N., Hirata N.,
740 Honda R., Honda C., Hosoda S., Iijima Y., Ikeda H., Ishiguro M., Ishihara Y., Iwata T.,
741 Kawahara K., Kikuchi S., Kitazato K., Matsumoto K., Matsuoka M., Michikami T.,
742 Mimasu Y., Miura A., Mori O., Morota T., Nakazawa S., Namiki N., Noda H., Noguchi
743 R., Ogawa N., Ogawa K., Okada T., Okamoto C., Ono G., Ozaki M., Saiki T., Sakatani
744 N., Sawada H., Senshu H., Shimaki Y., Shirai K., Sugita S., Takei Y., Takeuchi H., Tanaka
745 S., Tatsumi E., Terui F., Tsukizaki R., Wada K., Yamada M., Yamada T., Yamamoto Y.,
746 Yano H., Yokota Y., Yoshihara K., Yoshikawa M., Yoshikawa K., Fukai R., Furuya S.,
747 Hatakeda K., Hayashi T., Hitomi Y., Kumagai K., Miyazaki A., Nishimura M., Soejima
748 H., Iwamae A., Yamamoto D., Yoshitake M., Yada T., Abe M., Usui T., Watanabe S., and
749 Tsuda Y. 2022. A pristine record of outer Solar System materials from asteroid Ryugu's
750 returned sample. *Nature Astronomy* 6: 1163–1171. https://doi.org/10.1038/s41550-022-
751 01745-5

752 Kebukawa, Y., Alexander, C. M. O. D., & Cody, G. D. (2011). Compositional diversity in
753 insoluble organic matter in type 1, 2 and 3 chondrites as detected by infrared spectroscopy.
754 Geochimica et Cosmochimica Acta, 75(12), 3530–3541.
755 https://doi.org/10.1016/j.gca.2011.03.037

756 Kebukawa, Y., Kobayashi, H., Urayama, N., Baden, N., & Kondo, M. (2018). Nanoscale
757 infrared imaging analysis of carbonaceous chondrites to understand organic-mineral
758 interactions during aqueous alteration. *PNAS*, 1–6.
759 https://doi.org/10.1073/pnas.1816265116

760 Le Guillou, C., Bernard, S., Brearley, A. J., & Remusat, L. (2014). Evolution of organic matter
761 in Orgueil, Murchison and Renazzo during parent body aqueous alteration: In situ
762 investigations. *Geochimica et Cosmochimica Acta*, *131*, 368–392.
763 https://doi.org/10.1016/j.gca.2013.11.020

764 Madejová, J., Gates, W. P., & Petit, S. (2017). IR Spectra of Clay Minerals. *Developments in*
765 *Clay Science* (Vol. 8). https://doi.org/10.1016/B978-0-08-100355-8.00005-9

766 Mathurin, J., Dartois, E., & Dazzi, A. (2022). Nanometerscale infrared chemical imaging
767 (AFM-IR) study of Ryugu samples returned by the Hayabusa 2 space mission. In *53th*
768 *Lunar and Planetary Science Conference* (p. 2142).

769 Mathurin, Jeremie, Deniset-Besseau, A., Bazin, D., Dartois, E., Wagner, M., & Dazzi, A.
770 (2022). Photothermal AFM-IR spectroscopy and imaging: Status, challenges, and trends.
771 *Journal of Applied Physics*, *131*(1). https://doi.org/10.1063/5.0063902

772 Mathurin, J., Dartois, E., Pino, T., Engrand, C., Duprat, J., Deniset-besseau, A., Borondics, F.,
773 Sandt, C., Dazzi, A. (2019). Nanometre-scale infrared chemical imaging of organic matter
774 in ultra-carbonaceous Antarctic micrometeorites (UCAMMs). Astronomy &

Astrophysics, 160, 1–9.

Nakamura T., Matsumoto M., Amano K., Enokido Y., Zolensky M., E., Mikouchi T., Genda H., Tanaka S., Zolotov M. Y., Kurosawa K., Wakita S., Hyodo R., Nagano H., Nakashima D., Takahashi Y., Fujioka Y., Kikuiri M., Kagawa E., Matsuoka M., Brearley A. J., Tsuchiyama A., Uesugi M., Matsuno J., Kimura Y., Sato M., Milliken R. E., Tatsumi E., Sugita S., Hiroi T., Kitazato K., Brownlee D., Joswiak D. J., Takahashi M., Ninomiya K., Takahashi T., Osawa T., Terada K., Brenker F. E., Tkalcec B. J., Vincze L., Brunetto R., Aléon-Toppani A., Chan Q. H., S., Roskosz M., Viennet J-C., Beck P., Alp E. E., Michikami T., Nagaashi Y., Tsuji T., Ino Y., Martinez J., Han J., Dolocan A., Bodnar R. J., Tanaka M., Yoshida H., Sugiyama K., King A. J., Fukushi K., Suga H., Yamashita S., Kawai T., Inoue K., Nakato A., Noguchi T., Vilas F., Hendrix A. R., Jaramillo-Correa C., Domingue D. L., Dominguez G., Gainsforth Z., Engrand C., Duprat J., Russell S. S., Bonato E., Ma C., Kawamoto T., Wada T., Watanabe S., Endo R., Enju S., Riu L., Rubino S., Tack P., Takeshita S., Takeichi Y., Takeuchi A., Takigawa A., Takir D., Tanigaki T., Taniguchi A., Tsukamoto K., Yagi T., Yamada S., Yamamoto K., Yamashita Y., Yasutake M., Uesugi K., Umegaki I., Chiu I., Ishizaki T., Okumura S., Palomba E., Pilorget C. M., Potin S., Alasli A., Anada S., Araki Y., Sakatani N., Schultz C., Sekizawa O., Sitzman S. D., Sugiura K., Sun M., Dartois E., De Pauw E., Dionnet Z., Djouadi Z., Falkenberg G., Fujita R., Fukuma T., Gearba I. R., Hagiya K., Hu M., Y., Kato T., Kawamura T., Kimura M., Kubo M. K., Langenhorst F., Lantz C., Lavina B., Lindner M., Zhao J., Vekemans B., Baklouti D., Bazi B., Borondics F., Nagasawa S., Nishiyama G., Nitta K., Mathurin J., Matsumoto T., Mitsukawa I., Miura H., Miyake A., Miyake Y., Yurimoto H., Okazaki R., Yabuta H., Naraoka H., Sakamoto K., Tachibana S., Connolly Jr., H. C., Lauretta D. S., Yoshitake M., Yoshikawa M., Yoshikawa K., Yoshihara K., Yokota Y., Yogata K., Yano H., Yamamoto Y., Yamamoto D., Yamada M., Yamada T., Yada T., Wada K., Usui T., Tsukizaki R., Terui F., Takeuchi H., Takei Y., Iwamae A., Soejima H., Shirai K., Shimaki Y., Senshu H., Sawada H., Saiki T., Ozaki M., Ono G., Okada T., Ogawa N., Ogawa K., Noguchi R., Noda H., Nishimura M., Namiki N., Nakazawa S., Morota T., Miyazaki A., Miura A., Mimasu Y., Matsumoto K., Kumagai K., Kouyama T., Kikuchi S., Kawahara K., Kameda S., Iwata T., Ishihara Y., Ishiguro M., Ikeda H., Hosoda S., Honda R., Honda C., Hitomi Y., Hirata N., Hirata N., Hayashi T., Hayakawa M., Hatakeda K., Furuya S., Fukai R., Fujii A., Cho Y., Arakawa M., Abe M., Watanabe S., and Tsuda Y. (2023) Formation and evolution of carbonaceous asteroid Ryugu: Direct evidence from returned samples. *Science* 379: https://doi.org/science.eabn8671.

Noguchi, T., Matsumoto, R., Yabuta, H., Kobayashi, H., Miyake A., Naraoka. H., Okazaki, R., Imae, I, Yamaguchi, A., David Kilcoyne, A. L., Takeichi, Y., and Takahashi, Y. (2022) Antarctic micrometeorite composed of CP and CS IDP-like material: A micro-breccia originated from a partially ice-melted comet-like small body. Meteorit. Planet. Sci. 57: 2042-2062. doi: 10.1111/maps.13919.

Noguchi T., Matsumoto T., Miyake A., Igami Y., Haruta M., Saito H., Hata S., Seto Y., Miyahara M., Tomioka N., Ishii H. A., Bradley J. P., Ohtaki K. K., Dobrică E., Leroux H.,

Le Guillou C., Jacob D., de la Peña F., Laforet S., Marinova M., Langenhorst F., Harries D., Beck P., Phan T. H. V., Rebois R., Abreu N. M., Gray J., Zega T., Zanetta P-M., Thompson M. S., Stroud R., Burgess K., Cymes B. A., Bridges J. C., Hicks L., Lee M. R., Daly L., Bland P. A., Zolensky M. E., Frank D. R., Martinez J., Tsuchiyama A., Yasutake M., Matsuno J., Okumura S., Mitsukawa I., Uesugi K., Uesugi M., Takeuchi A., Sun M., Enju S., Takigawa A., Michikami T., Nakamura T., Matsumoto M., Nakauchi Y., Abe M., Arakawa M., Fujii A., Hayakawa M., Hirata N., Hirata N., Honda R., Honda C., Hosoda S., Iijima Y., Ikeda H., Ishiguro M., Ishihara Y., Iwata T., Kawahara K., Kikuchi S., Kitazato K. Matsumoto K., Matsuoka M., Mimasu Y., Miura A., Morota T., Nakazawa S., Namiki N., Noda H., Noguchi R., Ogawa N., Ogawa K., Okada T., Okamoto C., Ono G., Ozaki M., Saiki T., Sakatani N., Sawada H., Senshu H., Shimaki Y., Shirai K., Sugita S., Takei Y., Takeuchi H., Tanaka S., Tatsumi E., Terui F., Tsukizaki R., Wada K., Yamada M., Yamada T., Yamamoto Y., Yano H., Yokota Y., Yoshihara K., Yoshikawa M., Yoshikawa K., Fukai R., Furuya S., Hatakeda K., Hayashi T., Hitomi Y., Kumagai K., Miyazaki A., Nakato A., Nishimura M., Soejima H., Suzuki A. I., Usui T., Yada T., Yamamoto D., Yogata K., Yoshitake M., Connolly Jr., H. C., Lauretta D. S., Yurimoto H., Nagashima K., Kawasaki N., Sakamoto N., Okazaki R., Yabuta H., Naraoka H., Sakamoto K., Tachibana S., Watanabe S., and Tsuda Y. (2023) A dehydrated space weathered skin cloaking the hydrated interior of Ryugu. *Nature Astronomy* 7: 170–181.

Noguchi T., Matsumoto T., Miyake A., Igami Y., Haruta M., Saito H., Hata S., Seto Y., Miyahara M., Tomioka N., Ishii H. A., Bradley J. P., Ohtaki K. K., Dobrică E., Leroux H., Le Guillou C., Jacob D., de la Peña F., Laforet S., Mouloud B., Marinova M., Langenhorst F., Harries D., Beck P., Phan T. H. V., Rebois R., Abreu N. M., Gray J., Zega T., Zanetta P-M., Thompson M. S., Stroud R., Burgess K., Cymes B. A., Bridges J. C., Hicks L., Lee M. R., Daly L., Bland P. A., Smith W. A., McFadzean S., Martin P-E., Bagot P. A. J., Fougerouse D., Saxey D. W., Reddy S., Rickard W. D. A., Zolensky M. E., Frank D. R., Martinez J., Tsuchiyama A., Yasutake M., Matsuno J., Okumura S., Mitsukawa I., Uesugi K., Uesugi M., Takeuchi A., Sun M., E., Takigawa A., Michikami T., Nakamura T., Matsumoto M., Nakauchi Y., Abe M., Nakazawa S., Okada T., Saiki T., Tanaka S., Terui F., Yoshikawa M., Miyazaki A., Nakato A., Nishimura M., Usui T., Yada T., Yurimoto H., Nagashima K., Kawasaki N., Sakamoto N., Hoppe P., Okazaki R., Yabuta H., Naraoka H., Sakamoto K., Tachibana S., Watanabe S., and Tsuda Y. Mineralogy and petrology of fine-grained samples recovered from the asteroid (162173) Ryugu. Meteoritics and Planetary Science, this volume.

Orthous-Daunay, F. R., Quirico, E., Beck, P., Brissaud, O., Dartois, E., Pino, T., & Schmitt, B. (2013). Mid-infrared study of the molecular structure variability of insoluble organic matter from primitive chondrites. *Icarus*, *223*, 534–543. https://doi.org/10.1016/j.icarus.2013.01.003

Phan, V.T. H., Rebois, R., Beck, P., Quirico, E., Bonal, L., & Noguchi, T. (2022). Nanoscale mineralogy and organic structure in Orgueil (CI) and EET 92042 (CR) carbonaceous chondrites studied with AFM-IR spectroscopy. Meteoritics & Planetary Science, 57(1), 3–

21. https://doi.org/10.1111/maps.13773

Phan, V.T.H., Quirico, E., Beck, P., Le Brech, Y., Jovanovic, L., Le Guillou, C., … Raya, J. (2021). Infrared spectroscopy quantification of functional carbon groups in kerogens and coals: A calibration procedure. Spectrochimica Acta - Part A: Molecular and Biomolecular Spectroscopy, 259, 119853. https://doi.org/10.1016/j.saa.2021.119853

Phan, V.T.H., Rebois, R., Beck, P., Quirico, E., Noguchi, T., & Takase, M. (2023). Chemical Functional Characterization of Immature and Mature Coals at the Nanoscale by Atomic Force Microscopy-Based Infrared Spectroscopy (AFM-IR). International Journal of Coal Geology, 267. https://doi.org/10.2139/ssrn.4253550

Piani, L., Tachibana, S., Hama, T., Tanaka, H., Endo, Y., Sugawara, I., … Kouchi, A. (2017). Evolution of Morphological and Physical Properties of Laboratory Interstellar Organic Residues with Ultraviolet Irradiation. The Astrophysical Journal, 837(1), 35. https://doi.org/10.3847/1538-4357/aa5ca6

Potapov, A., Bouwman, J., Jäger, C., & Henning, T. (2020). Dust/ice mixing in cold regions and solid-state water in the diffuse interstellar medium. *Nature Astronomy*. https://doi.org/10.1038/s41550-020-01214-x

Quirico, E., Bonal, L., Montagnac, G., Beck, P., & Reynard, B. (2020). New insights into the structure and formation of coals, terrestrial and extraterrestrial kerogens from resonant UV Raman spectroscopy. Geochimica et Cosmochimica Acta, 282, 156–176. https://doi.org/10.1016/j.gca.2020.05.028

Quirico, E., Bonal L., Kebukawa Y., Amano, K., Yabuta H., Phan, V. T. H., Beck, P., Rémusat, L., Dartois, E., Engrand, C., Martins, Z., Bejach, L., Dazzi, A., Deniset-Besseau, A., Jean Duprat, J., Mathurin, J., Montagnac, G., Barosch, J., Cody, G. D., De Gregorio, B., Enokido, Y., Hashiguchi, M., Kamide, K., . Kilcoyne, D., Komatsu, M., Matsumoto, M., Mostefaoui, S., Nittler, L., Ohigashi, T., Okumura, T., Sandford, S., Shigenaka, M., Stroud, R., Suga, H., Takahashi, Y., Takeichi, Y., Tamenori, Y., Verdier-Paoletti, M., Wakabayashi, D., Yamashita, S., Nakamura, T., Naraoka, H., Noguchi, T., Okazaki, R., Yurimoto, H., Sakamoto, K., Tachibana, S., Watanabe, S., Tsuda, Y. Compositional heterogeneity of insoluable organic matter extracted from Hayabusa 2 samples. This volume

Stroud, R. M., Barosch, J., Bonal, L., Burgess, K., Cody, G. D., De Gregorio, B. T., Daly, L., Dartois, E., Dobrică, E., Duprat, J., Engrand, C., Harries, D., Ishii, H., Kebukawa, Y., Kilcoyne, A. D., Langenhorst, F., Lee, M.R., Nittler, L. R., Quirico, E., Remusat, L., Sandford, S., Yabuta, H., Abe, M., Abreu, N. M., Bagot, P. A. J., Beck, P., Bejach, L., Bland, P. A., Bradley, J. P., Bridges, J. C., Cymes, B. A., Dazzi, A., de la Peña, F., Deniset-Besseau, A., Enju, S., Enokido, Y., Frank, D. R., Gray, J., Haruta, M., Hashiguchi, M., Hata, S., Hicks, L., Igami, Y., Jacob, D., Kamide, K., Komatsu, M., Laforet, S., Leroux, H., Le Guillou, C., Martins, Z., Marinova, M., Martinez, J., Mathurin, J., Matsumoto, M., Matsumoto, T., Matsuno, J., McFadzean, S., Michikami, T., Mitsukawa, I., Miyake, A.,

Miyahara, M., Miyazaki, A., Montagnac, G., Mostefaoui, S., Nakamura, T., Nakato, A., Naraoka, H., Nakauchi, Y., Nakazawa, S., Nishimura, M., Noguchi, T., Ohtaki, K., Ohigashi, T., Okada, T., Okumura, S., Okumura, T., Okazakaki, R., Phan, T. H. V., Rebois, R., Sakamoto, K., Saiki, T., Saito, H., Seto, Y., Shigenaka, M., Smith, W., Suga, H., Sun, M., Tachibana, S., Takahashi, Y., Takeichi, Y. Takeuchi, A., Takigawa, A., Tamenori, Y., Tanaka, S., Terui, F., Thompson, M.S., Tomioka, N., Tsuchiyama, A., Tsuda, Y., Uesugi, K., Uesugi, M., Usui, T., Verdier-Paoletti, M., Wakabayashi, D., Watanabe, S., Yada, T., Yamashita, S., Yasutake, M., Yogata, K., Yoshikawa, M., Yurimoto, H., Zanetta, P. M. Zega, T., Zolensky, M. E. Electron microscopy observations of the diversity of Ryugu organic matter and its relationship to minerals at the micro-to-nanoscale. This volume.

Viennet, J-C. Roskosz, M., Nakamura, T., Beck, P., Baptiste, B., Lavina, B., Alp, E. E, Hu, M. Y., Zhao, J., Gounelle, M., Brunetto, R., Yurimoto, H., Noguchi, T., Okazaki, R., Yabuta, H., Naraoka, H., Sakamoto, K., Tachibana, S., Yada, T., Nishimura, M., Nakato, A., Miyazaki, A., Yogata, K., Abe, M., Okada, T., Usui, T., Yoshikawa, M., Saiki, T., Tanaka, S., Terui, F., Nakazawa, S., Watanabe, S., Tsuda, Y. (2023) Interaction between clay minerals and organics in asteroid Ryugu. Geochem. Persp. Lett. 25, 8–12. https://doi.org/10.7185/geochemlet.2307

Vollmer, C., Pelka, M. Leitner, J., Janssen, A. (2020a). Amorphous silicates as a record of solar nenular and parent body processes – A transmission electron microscope study of fine-grained rims and matrix in three Antarctic CR chondrites. Meteoritics & Planetary Science. 55(7), 1491-1508

Vollmer, C., Leitner, J., Kepaptsoglou, D., Ramasse, Q. M., King, A. J., Schofield, P. F., … Hoppe, P. (2020b). A primordial 15N-depleted organic component detected within the carbonaceous chondrite Maribo. *Scientific Reports*, *10*(1), 1–9. https://doi.org/10.1038/s41598-020-77190-z

Figures

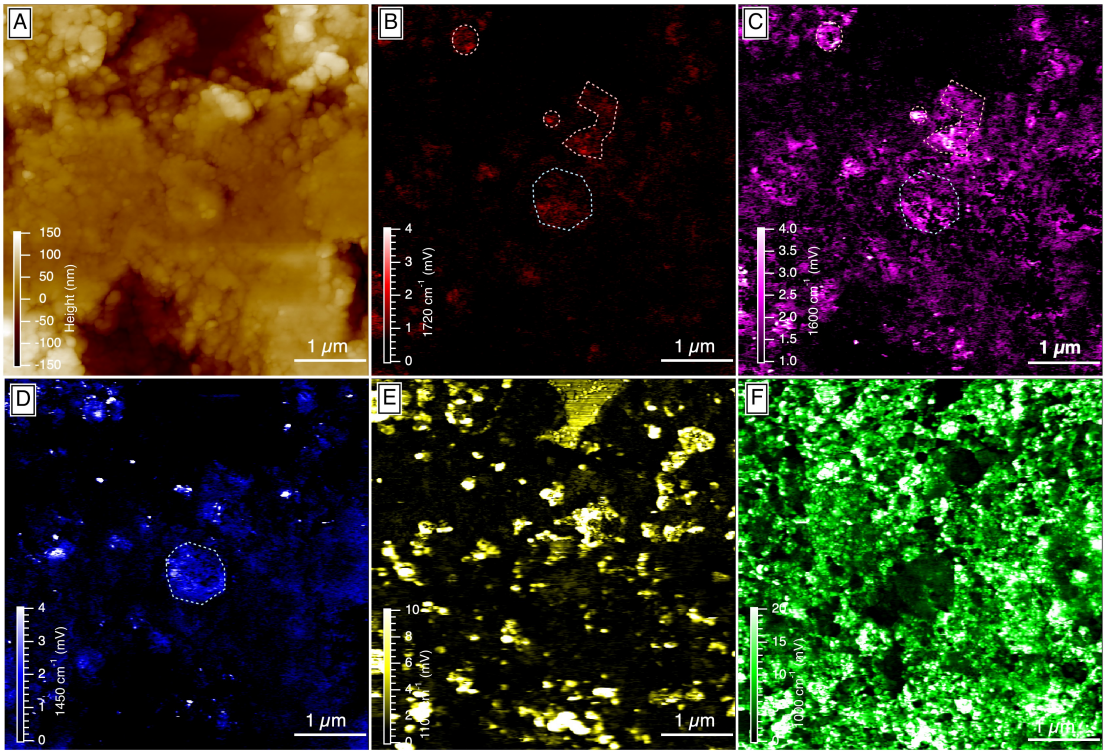

Figure 1. C0105-0032. (A) Topographic image (AFM) of the region of interest (ROI of 5 × 5 μm^2); Chemical images of the absorption band at (B) C=O at 1720 cm^{-1}, (C) C=C and/or water at 1600 cm^{-1}, (D) Carbonate and/or CH_2 bending mode at 1450 cm^{-1}, (E) SO_4 and/or wing of Si-O at 1100 cm^{-1} and (F) Si-O at 1000 cm^{-1}

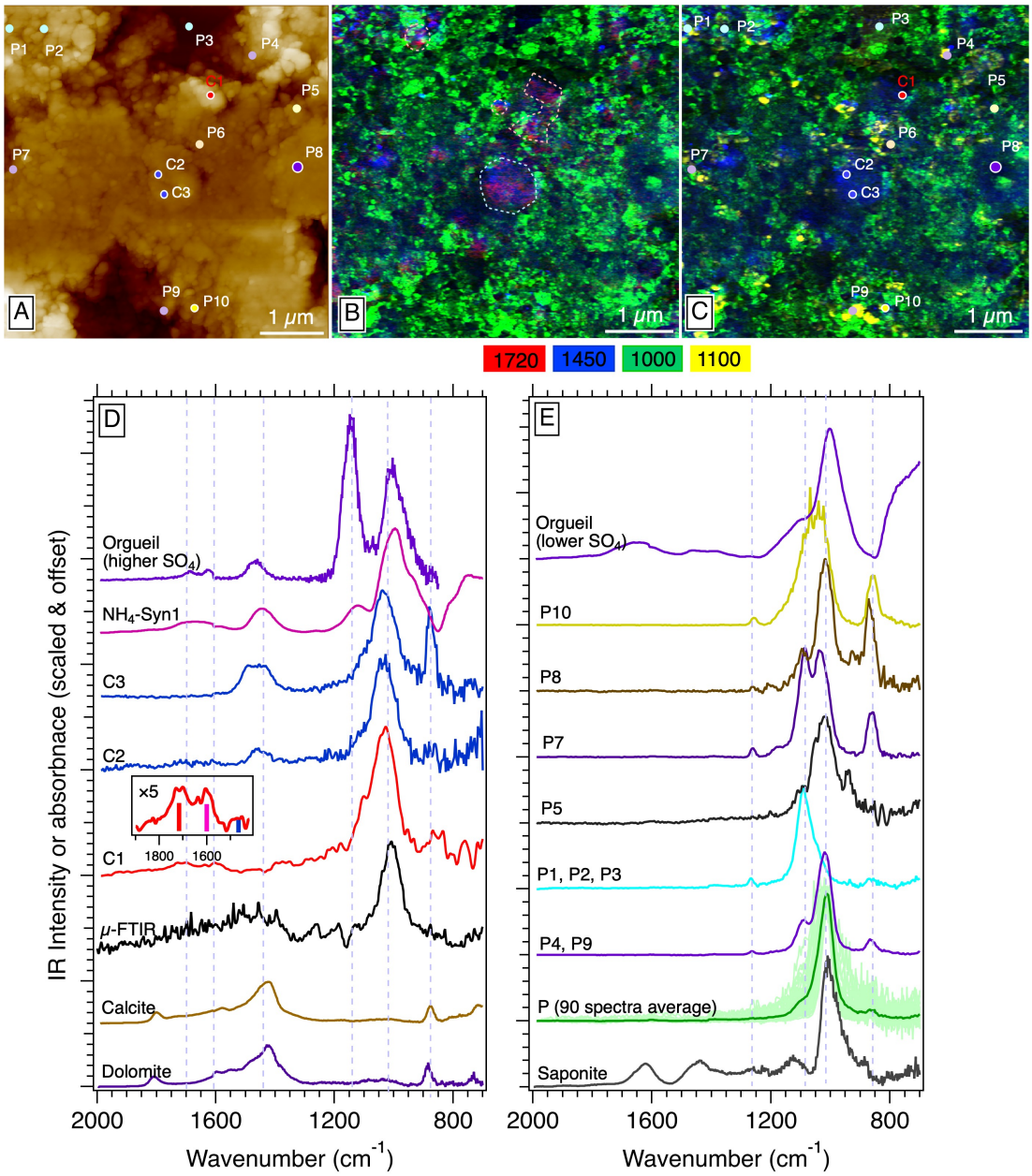

Figure 2. C0105-0032. (A) Topographic image (AFM) with the single-point AFM-IR spectral positions surrounding the 5 × 5 μm^2 image (labeled C1: red point, C2, C3: blue point, P1-P10); (B) A composite image at 1720, 1000 and 1450 cm^{-1}, (C) A composite image at 1450, 1000 and 1100 cm^{-1}; (D) Comparison between the single-point AFM-IR spectra in carbonate-rich regions and the average μ-FTIR spectrum of same Ryugu grain, AFM-IR spectra of carbonate references (dolomite, calcite) and NH_4-Syn-1 (*Ammonium-mica-montmorillonite*); the AFM-IR spectra of Orgueil with high sulfate; (E) Comparison between AFM-IR spectra of phyllosilicate-rich regions, AFM-IR spectra of saponite and Orgueil with lower sulfate.

941

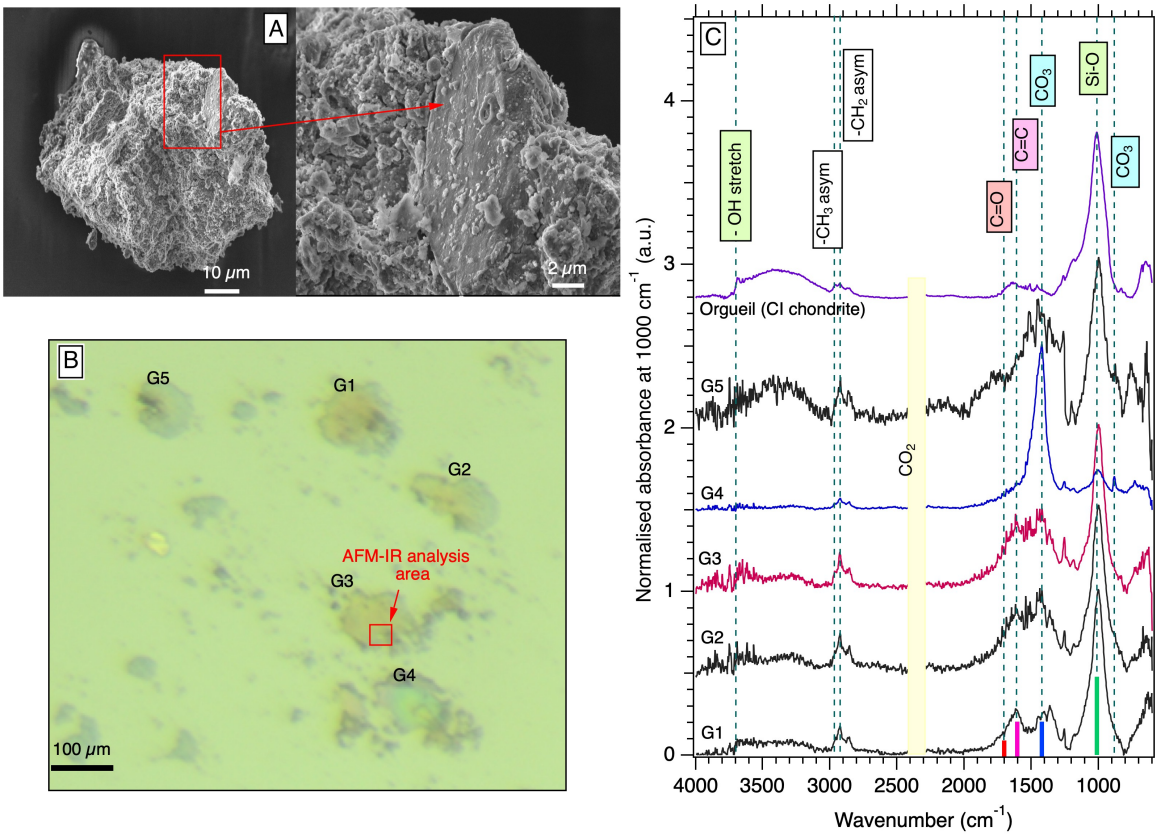

942

943 Figure 3. C0105-0038. μ-FTIR spectra of Ryugu sample in different grains. (A) Back scattered
944 electron (BSE) image showing the melted splash due to the space weathering (Noguchi et al.,
945 2023). (B) Visible image of different fractured grains after crushing between two diamond
946 windows (G1 – G5) for μ-FTIR analyze showing the location of the AFM-IR map (red square).
947 (C) Different μ-FTIR spectra corresponding to G1 – G5 grains in the visible image (B) in
948 comparison to μ-FTIR spectrum of Orgueil (CI chondrite).

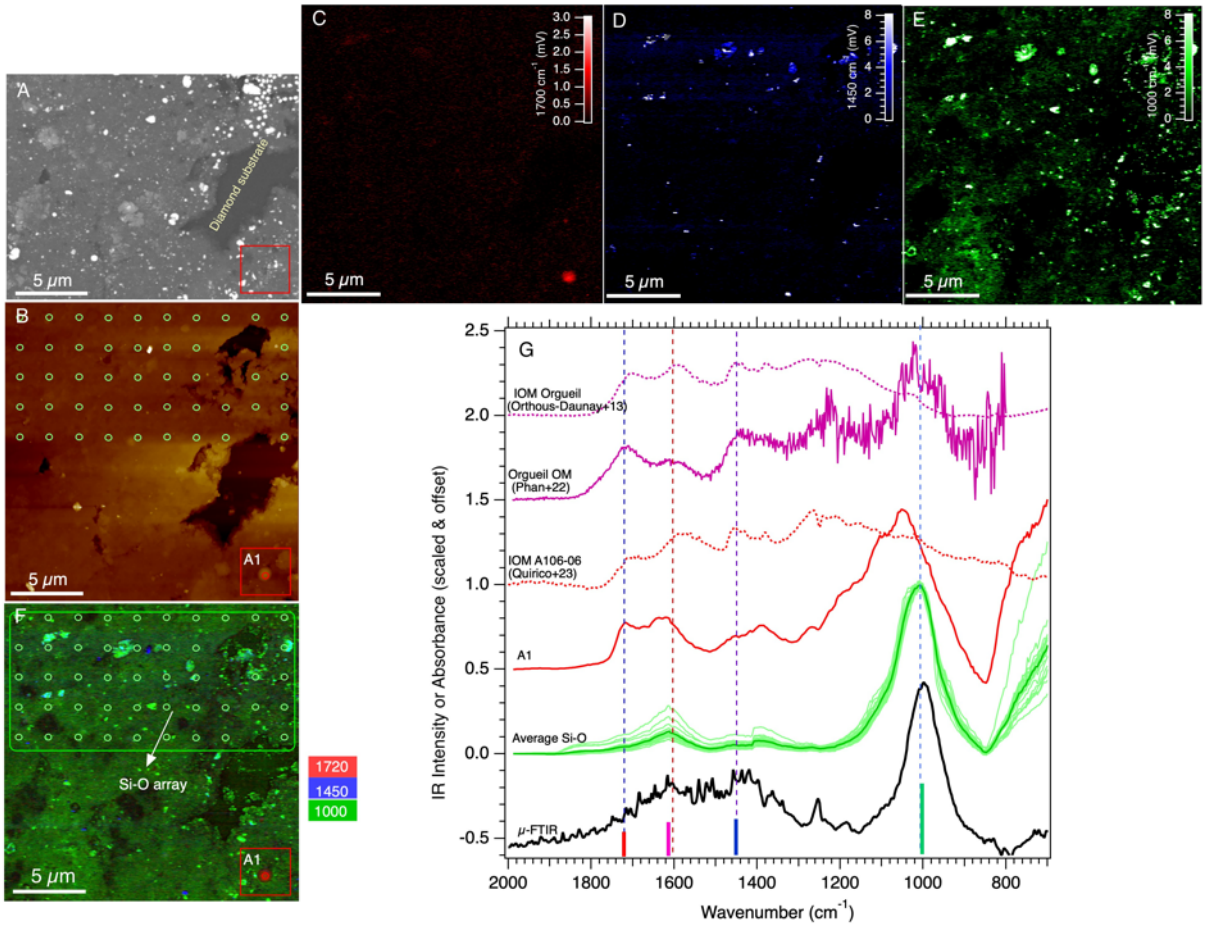

Figure 4. **C0105-0038 (20× 20 µm²)**. (A) SEM image showing the region of AFM-IR measurements using the APE laser in the 2000 – 700 cm^{-1} range. (B) Topographical image of the 20 × 20 μm^2 area. AFM-IR images collected at different absorption band at (C) C=O at 1720 cm^{-1} (in red); (D) Carbonate and/or CH_2 bend mode at 1450 cm^{-1} (in blue); (E) Si-O at 1000 cm^{-1} (in green) and (F) Composite RGB image in tapping mode of the three map: 1720, 1000 and 1450 cm^{-1}, respectively with a small organic globule are visible in red square surrounded by a dominant phyllosilicate in green; (G) Comparison between AFM-IR single point spectra in the locations shown in (B) and (F), the µ-FTIR spectrum of Ryugu G3 grain, IOM Ryugu A106-06 (Quirico et al., this volume), IOM Orgueil (Orthous-Daunay et al., 2013) and the AFM-IR spectra of organic particles in Orgueil (Phan et al., 2022).

961

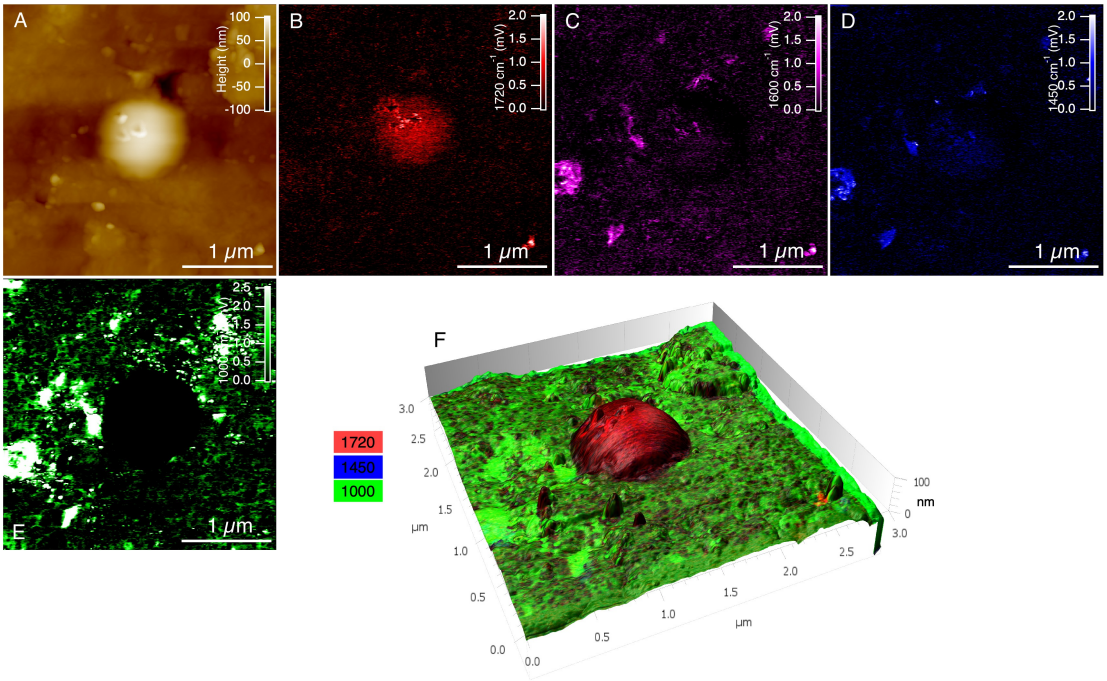

962

963 Figure 5. **C0105-0038 (3 × 3 µm²)**. (A) Topographical image (AFM) showing some small spots
964 damaged due to the physical contact of the AFM tip; Absorption images of the bands (B) C=O
965 at 1720 cm^{-1}; (C) C=C and water at 1600 cm^{-1}; (D) CO_3^{2-} / CH_2 bending mode at 1450 cm^{-1}; (E)
966 Si-O at 1000 cm^{-1}; (F) Composite 3D view of the RGB image derived from the three maps:
967 1720, 1000 and 1450 cm^{-1}, respectively, showing the "lentil" shape of the globule.

968

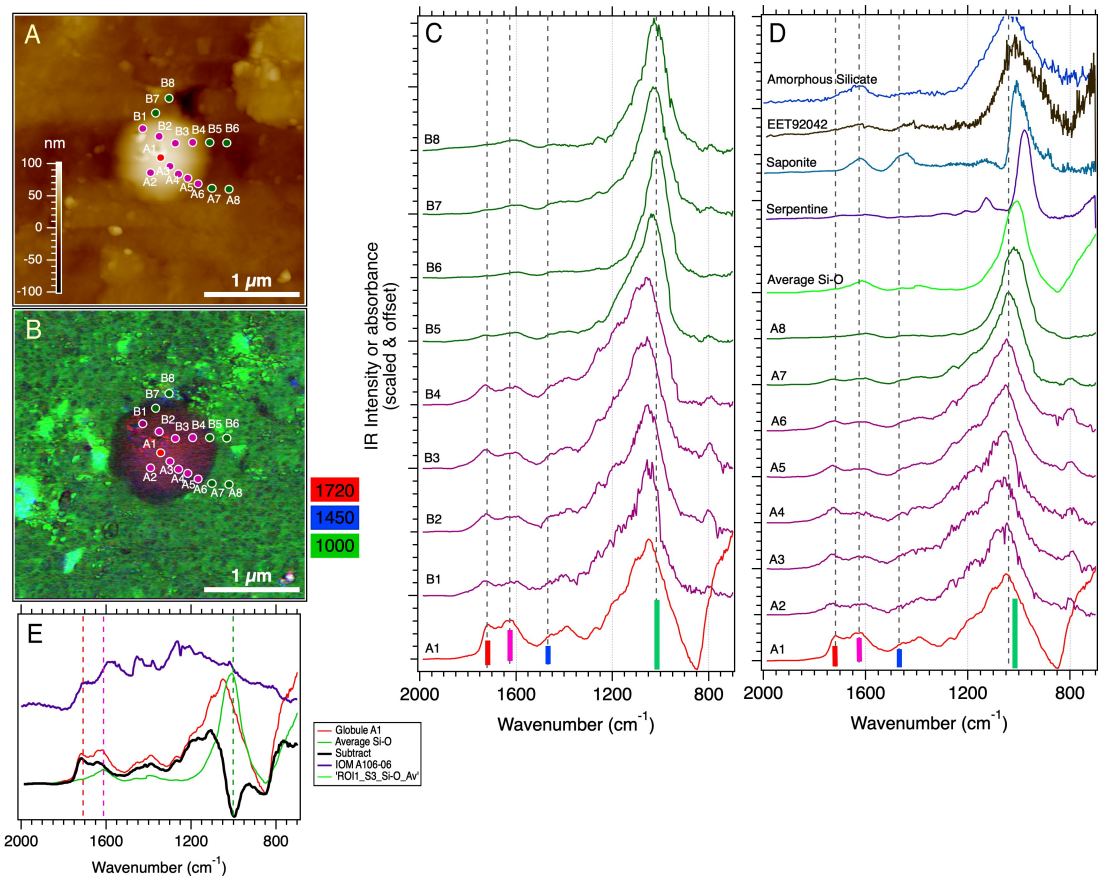

969

970 Figure 6. C0105-0038-G3. (A) AFM and (B) Composite 2D view of the RGB image derived
971 from three AFM-IR images at 1720 cm^{-1}, 1450 cm^{-1} and 1000 cm^{-1}, respectively with the
972 location of the single point AFM-IR spectra; (C) AFM-IR spectra performed in selected
973 positions indicated in images (A)-(B) images (labeled B1-B8); (D) the AFM-IR spectra
974 performed in selected positions shown on the (A)-(B) images (labeled A1-A8) from the centre
975 to exterior of the organic globule, in comparison with mixture of saponite and carbonate,
976 serpentine and amorphous silicate (anhydrous silicate) (Potapov et al., 2020) and AFM-IR
977 spectrum of amorphous silicate in carbonaceous chondrite EET 92042 (Phan et al., 2022); (E)
978 The subtracted spectrum between the organic globule (A1 spectrum) and the average Si-O
979 spectrum, in comparison with μ-FTIR spectrum of IOM A106-06 (Quirico et al., this volume).

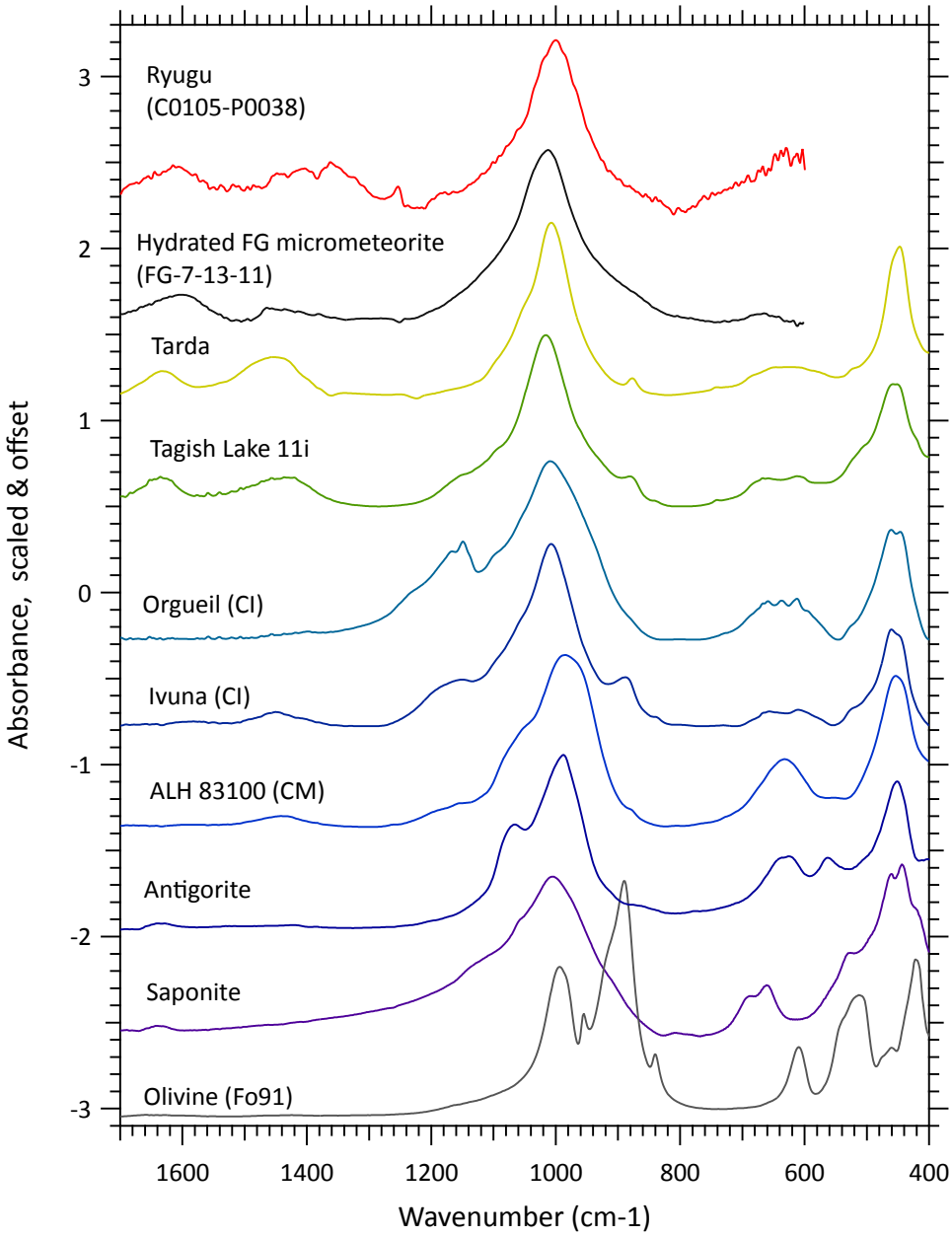

Figure 7. Comparison of the MIR spectra of Ryugu grain C0105-0038 to CI chondrites (Orgueil and Ivuna from Beck et al., 2014), ungrouped carbonaceous chondrites (Tarda and Tagish Lake from Gilmour et al., 2019), a CM chondrite and reference mineral phases (Beck et al., 2014).

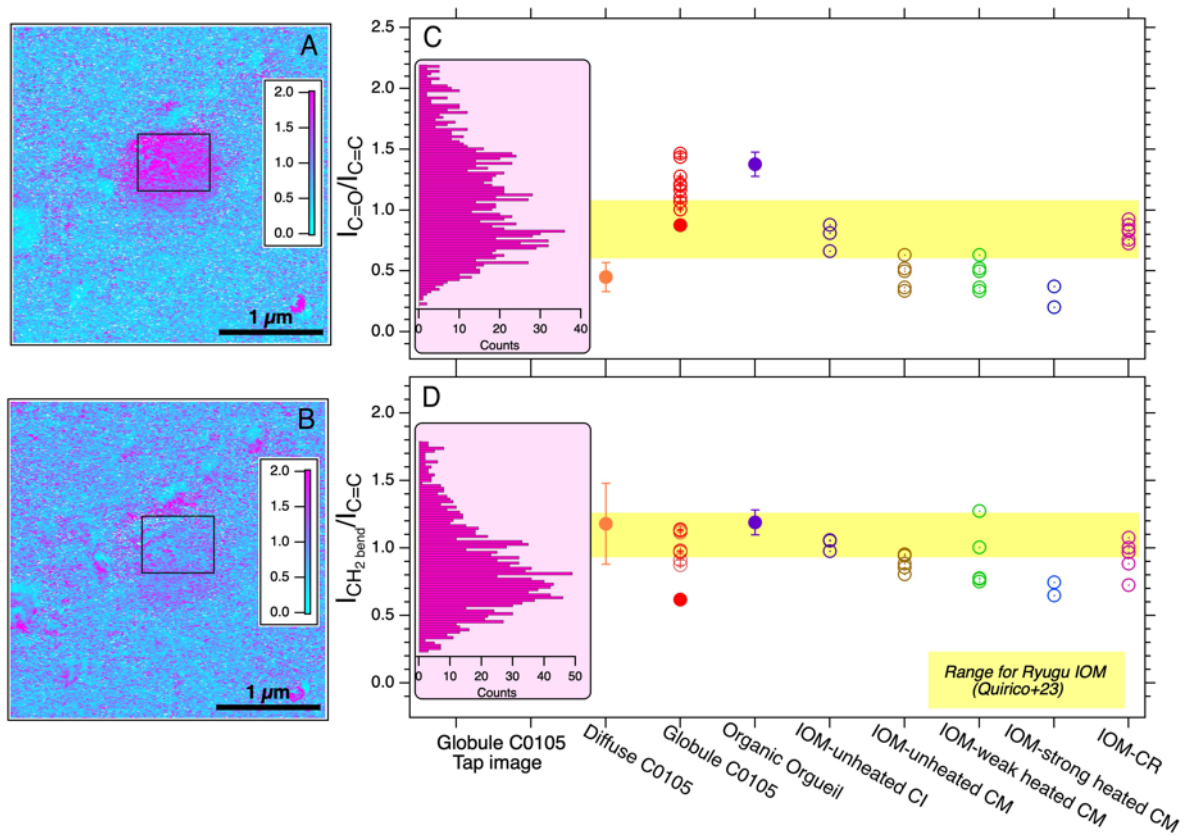

Figure 8. C0105-0038. The AFM-IR ratio images showing (A) the I_{1720}/I_{1600} and (B) I_{1450}/I_{1600} ratio of interest region (3×3 μm^2) for C0105-0038. Comparison of the peak intensity ratio of (C) C=O and C=C bands at 1720 and 1600 cm^{-1}, respectively and (D) CH_2 bending mode and C=C bands at 1450 and 1600 cm$^{-1,}$ respectively, including: Histogram of the I_{1720}/I_{1600} ratio extracted from (A), Histogram of the I_{1450}/I_{1600} extracted from (B), the contact AFM-IR spectra of the organic globule in "bulk" Ryugu in C0105-0038, the AFM-IR spectra of the organic particle in Orgueil (Phan et al., 2022); the μ-FTIR spectra of IOM-like Ryugu from Quirico et al. (this volume) in yellow bar, and the μ-FTIR spectra of various IOMs in carbonaceous chondrites (Quirico et al., 2018).